FEATURE ARTICLE

Recent advances in TiO₂-based photocatalysis

Hua Xu,[abc] Shuxin Ouyang,[abc] Lequan Liu,[c] Pakpoom Reunchan,[cd] Naoto Umezawa[ace] and Jinhua Ye*[abc]

Semiconductor photocatalysis is a promising approach to combat both environmental pollution and the global energy shortage. Advanced TiO₂-based photocatalysts with novel photoelectronic properties are benchmark materials that have been pursued for their high solar-energy conversion efficiency. In general, the photocatalytic efficiency is affected by the degree of light absorption, charge separation, and surface reactivity. Consequently, in this review we first discuss a series of interesting studies that aim to extend the light absorption of TiO₂ from UV wavelengths into the visible or even the near-infrared region. We next focus on attempts to overcome the drawback that dopants usually act as charge recombination centres. We discuss the use of either selective local doping or the introduction of disorder together with doping, which aims to facilitate charge separation while preserving the visible-light response. We also show that crystal facet engineering can endow TiO₂ with superior physicochemical properties, thus yielding high surface reactivity in photocatalytic reactions. Finally, we examine the recent theoretical advances of TiO₂-based photocatalysis.

aTU-NIMS Joint Research Center, Tianjin Key Laboratory of Composite and Functional Materials, School of Materials Science and Engineering, Tianjin University, 92 Weijin Road, Nankai District, Tianjin 300072, P. R. China

bCollaborative Innovation Center of Chemical Science and Engineering (Tianjin), Tianjin 300072, P.R. China

cEnvironmental Remediation Materials Unit, and International Center for Materials Nanoarchitectonics (WPI-MANA), National Institute for Materials Science, 1-1 Namiki, Tsukuba 305-0044, Japan. E-mail: Jinhua.YE@nims.go.jp

dDepartment of Physics, Faculty of Science, Kasetsart University, Bangkok 10900, Thailand

ePRESTO, Japan Science and Technology Agency (JST), 4-1-8 Honcho Kawaguchi, Saitama 332-0012, Japan

Hua Xu was awarded a PhD in Chemistry from Hokkaido University, Sapporo, Japan in 2013, under the guidance of Prof. Jinhua Ye. After graduation, she worked as a lecturer in the TU-NIMS Joint Research Center, School of Material Science and Engineering, Tianjin University, Tianjin, China. Her research interests are synthesis and characterization of novel TiO₂-based photocatalysts for application in solar-to-energy conversion.

Shuxin Ouyang received his BSc degree from the Nanjing University in 2004 and his PhD degree in Materials Science from Nanjing University in 2009 under the supervision of Prof. Zhigang Zou and Prof. Jinhua Ye. Since 2009, he worked in Prof. Ye's group as a post-doctoral fellow at the National Institute for Materials Science (NIMS), Japan. From 2014, he joined the TU-NIMS Joint Research Center of Tianjin University, China, and was appointed as an Associate Professor. He is interested in developing and fabricating new photocatalysts, electronic structures of semiconductor photocatalysts, and surface/interface engineering of photocatalysts.

1. Introduction

Photocatalysis is a promising, environmentally friendly technology for the conversion of solar energy into chemical energy.[1–4] Potential applications include photodegradation of hazardous substances,[5,6] photocatalytic water splitting,[7–10] artificial photosynthesis,[11–13] photo-induced super-hydrophilicity,[14] and photoelectrochemical conversion.[15] To date, a wide variety of semiconductors have been investigated as photocatalysts in addition to traditional materials such as TiO_2,[16–21] WO_3,[22–24] CdS,[24–26] and $SrTiO_3$.[27,28] Novel photocatalysts are still being discovered; recent reports include Ag_3PO_4,[29,30] C_3N_4,[31–33] and metal–organic framework (MOF) based materials.[34–36] However, TiO_2 remains the most popular material and can be considered as a benchmark in the field of photocatalysis.[37–39] The many advantages of TiO_2 include high photoreactivity, good stability with time, low cost, and environmentally friendly nature. In Japan, TiO_2 has been used in air purifiers and self-cleaning windows since the late 1990s.[40–43] More commonly, TiO_2 has been used as a white pigment from ancient times, and thus its safety for both humans and the environment is guaranteed by history.[44]

The evolution of TiO_2-based photocatalysis can be traced back to the early 1930s. In 1938, Doodeve et al. reported that active oxygen species produced on the TiO_2 surface can bleach dyes under UV light irradiation; TiO_2 was referred to as a "photosensitizer" in that publication.[45] The first researchers to use the terminology "photocatalyst" with respect to TiO_2 might be Kato and Mashio in 1956, whose report is entitled "Autooxidation by TiO_2 as a photocatalyst".[44] In their experiments, the autooxidation of organic solvents and the simultaneous formation of H_2O_2 were observed under the irradiation of a Hg lamp. In 1972, Fujishima and Honda reported the landmark discovery of water photolysis on a TiO_2 electrode,[37] which aroused much attention towards TiO_2-based photocatalysis. As shown in Fig. 1, the number of publications related to this topic

Lequan Liu received his PhD degree in 2011 from Lanzhou Institute of Chemical Physics, Chinese Academy of Sciences under the supervision of Prof. Youquan Deng. In the same year, he moved to NIMS (Japan) as a postdoctoral fellow in Prof. Jinhua Ye's group. His research interests involve noble metal catalysis and developing metal@semiconductor composite materials for artificial photosynthesis.

Naoto Umezawa completed the doctoral course in the Department of Physics, University of Tokyo Graduate School of Science, and was employed as a Postdoctoral Scientist at the University of Southern California in 2003. He joined NIMS as a Special Researcher in 2004 and was appointed to his present position as a Senior Researcher at NIMS in 2008. In 2007, he was a Visiting Scientist at the University of California at Santa Barbara. He also received the 29th Japan Society of Applied Physics Best Original Paper Award in 2007. His research field is materials design using first-principles calculation.

Pakpoom Reunchan has received his PhD from Suranaree University of Technology (SUT), Thailand under the supervision of Prof. Sukit Limpijumnong in 2009. After working at the Asia Pacific center for Theoretical Physics (APCTP) in Korea and NIMS in Japan as a postdoctoral fellow during 2009–2012, he has joined the Department of Physics, Faculty of Science, Kasetsart University, Thailand. His background is electronic structure calculations of real materials, focusing on defects in semiconductors. His current research interests are computational design of highly active photocatalysts based on doping schemes and hydrogen storage materials.

Jinhua Ye received her PhD from the University of Tokyo in 1990, and joined the National Research Institute for Metals (former organization of NIMS) in 1991. She is now the director of the Environmental Remediation Materials Unit, and a Principle Investigator at the International Center for Materials Nanoarchitectonics (MANA), NIMS. She is also an appointed director of the TU-NIMS Joint Research Center, and a Professor of Materials Science at Tianjin University, China, since 2011. Her current research interests focus on the research and development of photo-functional materials and their applications in the fields of environment remediation and new energy production.
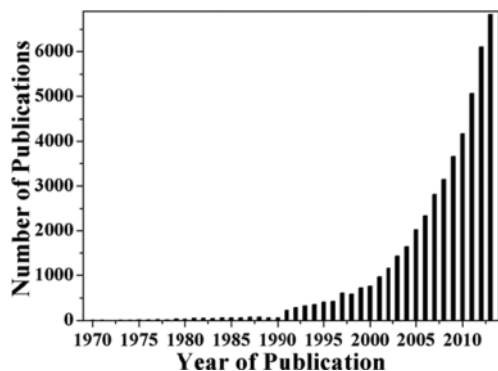
This journal is © The Royal Society of Chemistry 2014

J. Mater. Chem. A, 2014, **2**, 12642–12661 | **12643**

Fig. 1 Annual number of publications (Science Citation Index Expanded) in Web of Science when a search for the topic "titanium dioxide or titania or TiO_2" and "photo*" is performed.

steadily increased in the 1970s and 1980s, then grew exponentially since 1990s till now, indicating that TiO_2 is really a hot subject in the field of photocatalysis. It is also interesting to point out that studies based on TiO_2 have become more intensive over the last ten years.

The main topic of investigation has become concentrated on how to improve the solar energy conversion efficiency to meet engineering requirements. In general, a photocatalytic reaction consists of three steps as shown in Fig. 2. First, photoexcitation generates electrons (e^-) and holes (h^+). Next, the electrons and holes migrate to the TiO_2 surface. Finally, the electrons and holes react with adsorbed electron acceptors and donors, respectively, to complete the photocatalytic reaction.[4] Accordingly, much effort is currently focused on how to improve the light absorption, charge separation, and surface reactivity of TiO_2 in order to achieve outstanding photocatalytic performance.[46–50]

Both spatial structuring of TiO_2 to increase the effective path length of incident light[51] and band structure engineering to enhance the optical response in the UV to visible light range[17,52] can induce TiO_2 to absorb more photons. Attempts have been made to apply both physical concepts and spatial structuring to TiO_2, such as utilizing the slow-light effect in periodic TiO_2 photonic crystals,[53] the multi-reflection effect in semi-hollow TiO_2 spheres,[54] and Mie's scattering effect in TiO_2 spheres of particular size;[55] all of these interesting studies revealed that well-designed nanostructures can trap photons and force them to propagate more effectively through TiO_2, thus resulting in more efficient light absorption. A limitation of TiO_2 is its 3.2 eV

bandgap, which allows only UV light to be absorbed ($\lambda < 387$ nm, accounting for 5% of the solar spectrum). To harvest visible light (43% of the solar spectrum) for better solar energy conversion, it has been reported that either the inter-particle electronic coupling of TiO_2 nanocrystals[56] or localized surface plasmon resonance (LSPR) photosensitization[57] can be utilized. Chemical doping is also an effective method to enable visible light photocatalytic performance, by narrowing the bandgap of TiO_2. The prerequisite is that the integrity of the TiO_2 crystal structure should be maintained when pursuing the favourable modulations in the electronic structure.[58,59] Generally, the metal dopants (Cr,[60] Mn,[61] Fe,[62] Ni,[63] Cu,[64] etc.) substitute the Ti atoms and their states can mix with the conduction band or valence band, and in some cases can insert a new band into the original bandgap of TiO_2; while the non-metal dopants (C,[65] N,[17,66] F,[67,68] S,[69] Cl,[70] etc.) are introduced onto the O sites to mostly modulate the valence band of TiO_2.

After excitation by light, the photo-generated electrons and holes migrate to the surface. For TiO_2 electrodes, the existing electric field in the depletion region facilitates charge separation, hence this depletion region contributes most of the electrons and holes that are available for the photocatalytic reaction. However, doping can directly increase the carrier density and result in a narrower depletion region, which greatly hinders the electron–hole separation process.[71–74] In addition, surface dopants generally act as charge recombination centres.[75] These drawbacks greatly limit the practical use of doped TiO_2. Conversely, the selective doping of an inner region of a TiO_2 sample while keeping the outer region pure is a strategy that not only enables visible-light harvesting but also preserves a wide depletion region for efficient charge transfer, offering a promising and general way to enhance the photocatalytic efficiency.[76,77] Furthermore, disorder can be introduced on the surface layer of nanophase TiO_2 powder to obtain "black TiO_2", an approach that is different from conventional doping. The stable lower-energy mid-gap states that result from the surface disorder can localize both photo-excited electrons and holes and thus avoid fast recombination.[20] Therefore, appropriate modification is necessary to further fine-tune the local electronic structure of doped TiO_2 and achieve better charge separation.

Surface chemistry plays an important role in photocatalytic reactions because a variety of physical and chemical processes (e.g., adsorption of reactant molecules, surface transfer of photoexcited electrons to reactant molecules, and desorption of product molecules) take place on the surface.[19,78,79] The type
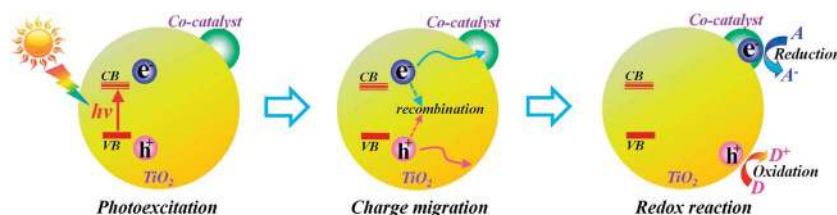

Fig. 2 Schematic picture of the TiO_2 photocatalytic reaction process.

of atomic arrangement and coordination on a surface influences the surface energy and reactivity. In general, the presence of more under-coordinated atoms on the surface will yield a higher surface energy; however, a higher surface energy does not directly imply superior surface reactivity.[80] The surface reactivity is determined by both the surface atomic structure and electronic structure. Much effort has been applied to the growth of TiO$_2$ single crystals with highly active surfaces exposed (*e.g.* the {100},[81,82] {001},[83,84] and {111} facets[85]); these studies have shown that the photocatalytic activity of TiO$_2$ differs with the type of facet exposed.[78] The surface adsorption/desorption ability and the redox potential of the charge carriers are influenced by the percentage of each facet exposed,[82] the surface area,[84] the coordination of surface atoms,[85] the concentration of surface oxygen vacancies,[30] and the facet-dependent electronic band structure.[80,86] All of these factors should be analysed together in facet engineering studies.[78,87]

In this article, we aim to bring the reader up to date regarding recent progress in TiO$_2$-based photocatalysis. Firstly, we introduce methods that have been adopted to enhance the light absorption of TiO$_2$, such as applying a physical concept (Mie's scattering) to TiO$_2$ spheres to reinforce the intrinsic optical absorption, utilizing electronic coupling in assemblies of TiO$_2$ nanocrystals to achieve a visible-light-response, and the use of LSPR-based Au-photosensitization for visible/near-infrared light harvesting. Then, approaches for obtaining better charge separation and overcoming the shortcomings of doping will be reviewed, such as selectively doping the inner layers of TiO$_2$ films, constructing p–n junctions in bulk TiO$_2$, and introducing surface disorder for better localization of photoexcited charge carriers. Thirdly, a systematic investigation of facet engineering in TiO$_2$ will be discussed. Finally, we focus on related theoretical studies that aim to provide a comprehensive understanding of TiO$_2$-based photocatalysis. This article provides a survey of recent advances in TiO$_2$ photocatalysis, and discusses effective solutions to the challenges in this field.

2. Light harvesting: from UV to visible to near-infrared light

The first step in photocatalysis is photoexcitation, thus highly efficient light harvesting is an important goal. To date, remarkable progress has been made to improve the absorption of light in TiO$_2$ materials, not only in the intrinsic absorption region of TiO$_2$, but also to extend the spectral range into the visible/near infrared region. Light absorption can be improved by applying physical concepts to spatially nanostructured TiO$_2$ to increase the effective optical path length through the material. Doping TiO$_2$ with other elements, which introduce impurity levels between the conduction band and valence band, is a general method to extend the optical sensitivity to the visible light region. Alternatively, making use of electronic coupling between two TiO$_2$ nanocrystals in close proximity, in order to engineer the electronic band structure and obtain a self-narrowed bandgap without changing the chemical composition, is also a promising route towards enhanced solar energy

utilization. Another versatile method of extending the optical response of TiO$_2$ to the visible or even the near-infrared region is to utilize photosensitization.

2.1 Physical concepts applied to spatially structured TiO$_2$

When a TiO$_2$ photocatalyst is illuminated, light can be absorbed, reflected, or scattered. We assume that only the absorbed photons can generate electrons and holes. Nevertheless, it is obvious that the path length of the incident light varies with different TiO$_2$ nano-architectures. If physical concepts such as the slow-light effect[22,88,89] or Mie's scattering effect[90–92] are applied to TiO$_2$ with optimized spatial structuring, the light can be forced or guided to reflect/scatter many times as it passes through the material; in this case, the effective optical path length is greatly increased, which offers more opportunities for photons to be absorbed by TiO$_2$ and ensures more efficient light harvesting in the photocatalytic reaction.

The slow-light effect in TiO$_2$ photonic crystals is a well-studied phenomenon that can lead to higher light absorption for photocatalysis.[51] In photonic crystals, the unique periodic dielectric structure can give rise to multiple diffraction and reflection and trap light inside the material;[53,89,93,94] this is similar to the way in which electron motion is affected by the periodic potential of semiconductor crystals. In the same way as a semiconductor crystal possesses an electronic bandgap, a photonic bandgap can be defined in a photonic crystal.[95] Bragg diffraction can prevent light with energy close to the photonic bandgap from propagating in a particular crystallographic direction. Therefore, light propagates through the material with a strongly reduced group velocity, leading to the delay and storage of light inside the photonic crystal, the so-called slow-light effect.[96] When the wavelength of the slow photons overlaps with the absorption regime of TiO$_2$ ($\lambda < 387$ nm), light absorption will be strongly promoted.[97] Bragg's equation implies that the slow-light wavelength can be tuned by controlling the pore size of the photonic crystal.[10,63,93] Experimentally, Ozin *et al.* fabricated TiO$_2$ inverse opal photonic crystals with various pore sizes to obtain photonic bandgaps centred at 280, 300, 325, 345, 370, 430, and 500 nm. When testing the photocatalytic properties *via* the photooxidation of adsorbed MB, it was demonstrated that more efficient photodegradation was achieved when the energy of the slow photons was close to the electronic bandgap of TiO$_2$.[53]

Nevertheless, it is worth noting that although the slow-light effect results from the periodicity of the photonic crystal structure, any disorder might break the integrity of the structure and lead to deterioration of the optical response.[98] To date, photonic crystals have mainly been fabricated in the form of films rather than powders, because crushing or grinding the material will destroy the periodicity of the structure. Thus, most applications of photonic crystals are limited to the photodegradation of hazardous substances[53,93,98] or to photoelectrochemical conversion.[22] To solve this problem, we have recently applied another physical concept, "Mie's scattering", to TiO$_2$ spheres in order to enhance the light utilization efficiency in photocatalytic water splitting.[55]

This journal is © The Royal Society of Chemistry 2014

J. Mater. Chem. A, 2014, **2**, 12642–12661 | **12645**

Mie's scattering is an optical phenomenon that occurs when the size of the spheres is comparable to the wavelength of the incident light. The light is strongly scattered in the forward direction, producing a pattern like an antenna lobe, with a sharper and more intense forward lobe (Fig. 3a).[90] Therefore, the path length of the incident light between neighbouring spheres is increased, leading to greater light utilization efficiency.[99] Theoretically, for an incident light wavelength λ, the scattering of a system that consists of dispersed spherical particles can be fully described by the radius of the spheres r and the complex refractive index m. The complex Mie coefficients a_n and b_n can be obtained from the complex Bessel–Riccatti functions ψ and ζ as follows:[91,92]

$$a_n = \frac{\psi'_n(mx)\psi_n(x) - m\psi_n(mx)\psi'_n(x)}{\psi'_n(mx)\zeta_n(x) - m\psi_n(mx)\zeta'_n(x)} \tag{1}$$

$$b_n = \frac{m\psi'_n(mx)\psi_n(x) - \psi_n(mx)\psi'_n(x)}{m\psi'_n(mx)\zeta_n(x) - \psi_n(mx)\zeta'_n(x)} \tag{2}$$

$$Q_{Sca} = \frac{2}{x^2} \sum_{n=1}^{\infty} (2n+1)\left(|a_n|^2 + |b_n|^2\right) \tag{3}$$

here the size parameter x is given by $x = 2\pi r/\lambda$, and Q_{Sca} is the Mie coefficient. Therefore, the light scattering efficiency is largely dependent on the size of the scattering spheres and the wavelength of the incident light.[91,92]

In our study, TiO$_2$ spheres with various diameters in the range 330–750 nm were fabricated in a controlled fashion to investigate the relationship between size and scattering properties. As shown in Fig. 3b, the positions of the scattering resonant peaks, which indicate highly efficient scattering in different wavelength regimes, were largely dependent on the size of the TiO$_2$ spheres. Resonant peaks were observed at 366, 400, and 440 nm for the T380, T450, and T600 samples,

respectively. The bandgap of TiO$_2$ is 3.2 eV, and thus the excitation of carriers can only be achieved by light with wavelengths smaller than 387 nm. Light is first scattered, then transferred to and absorbed by neighbouring TiO$_2$ spheres. The path length of the incident light is thus increased, resulting in higher light utilization efficiency for the 380 nm spheres. However, the effect of scattering for the 450 and 600 nm spheres is beyond the light absorption region of TiO$_2$, and thus is limited to the promotion of light harvesting.[55] Accordingly, the T380 sample exhibited significant photocatalytic activity for H$_2$ evolution that was approximately 5 and 3 times higher than that of the T450 and T600 samples, respectively (Fig. 3c).[55] Our study thus demonstrated that Mie's scattering can be adopted for the light absorption region of TiO$_2$ via morphological modulation to improve light harvesting, which results in excellent photocatalytic performance for H$_2$ evolution. Mie's scattering is a common natural phenomenon; for example, it is the reason why clouds look white because in the atmosphere, dust particles with various sizes can scatter all wavelengths of visible light. This study provides a promising and general way to effectively enhance light absorption in other semiconductor photocatalysts, simply by optimizing the diameters of the spheres and inducing Mie's scattering in their intrinsic light absorption regions.

2.2 Electronic coupling

The large bandgap of TiO$_2$ limits its absorption to UV light only, although visible light (400–700 nm) accounts for a much larger proportion (43%) of the solar spectrum. Electronic coupling, which is a general phenomenon in assemblies of TiO$_2$ nanocrystals, allows the bandgap to be narrowed and enables visible light absorption. In assemblies of nanoparticles, inter-particle coupling of the surface electrons (excitons), plasmons or
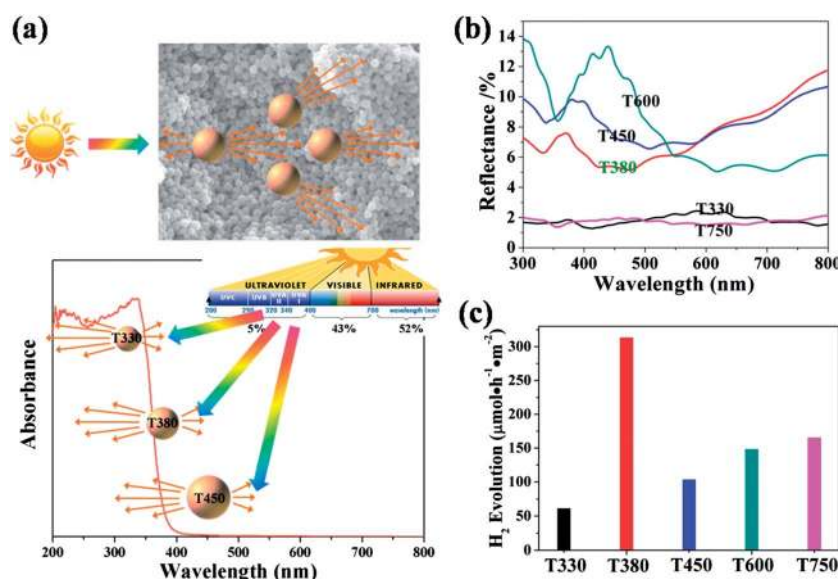

Fig. 3 (a) Schematic illustration of Mie's scattering. (b) Scattering resonance spectra of TiO$_2$ suspensions with various particle sizes. (c) Photocatalytic evolution of H$_2$ using TiO$_2$ sphere samples. TiO$_2$ spheres with diameters of 330, 380, 450, 600, and 750 nm are denoted as T330, T380, T450, T600, and T750, respectively. Reproduced with permission from ref. 55 (copyright 2012 American Chemical Society).

12646 | J. Mater. Chem. A, 2014, 2, 12642–12661

This journal is © The Royal Society of Chemistry 2014

magnetic moments may endow the particles with novel properties.[100,101] Exciton energy transfer and electronic coupling are the main types of interactions that have been considered in such assemblies, but they occur under different conditions in practical applications. Previous studies have revealed that when CdTe nanoparticles are separated by distances between 2 and 10 nm, long-range dipole–dipole interactions play an important role in inducing resonance energy transfer.[102] However, if the inter-particle separation is less than 2 nm, the wave functions of adjacent nanoparticles overlap; such electronic coupling results in a substantial alteration of the electronic structure and the observation of a red-shifted light absorption band and a photoluminescence emission band.[103] As shown in Fig. 4a, when a pair of nanoparticles is electronically coupled, bonding and anti-bonding levels are formed, resulting in a modified electronic structure.[56,104]

We performed a study on the effect of Ti–Ti electronic bonding in an assembly of anatase TiO_2 nanoparticles with an average size of 5 nm (Fig. 4b). The as-prepared sample of assembled nanoparticles had a bright yellow colour (inset of Fig. 4c) and a much narrower bandgap than bulk TiO_2, allowing the absorption of visible light up to 500 nm (Fig. 4c). However, when the sample was mechanically crushed to form powder, the colour returned to white because the interactions between neighbouring nanoparticles were eliminated. X-ray photoelectron spectroscopy (XPS) offered powerful evidence for the presence of such interactions; as shown in Fig. 4d, compared to the crushed sample, the Ti 2p peaks in the TiO_2 assembly sample were shifted to higher binding energy, indicating that interfacial Ti–Ti electronic bonding between the assembled TiO_2 nanocrystals was indeed present.[56] Most significantly, as shown in Fig. 4e, the assembled TiO_2 nanocrystals exhibited considerable activity in the visible light ($\lambda > 420$ nm, 300 W Xe

lamp with a 440 nm cut-off filter) region for the decomposition of isopropyl alcohol (IPA), whereas the crushed powder sample was inactive; this implies that the bandgap narrowing induced by the TiO_2 assembly can indeed enhance solar energy utilization. This finding opens up a new way to narrow the bandgaps of semiconductor photocatalysts via electronic coupling in nanoparticle assemblies.

2.3 Localized surface plasmon resonance photosensitization

The utilization of LSPR based photosensitization enables TiO_2 to absorb visible or even near-infrared light.[105,106] For plasmonic metals (such as Au,[107–112] Ag,[113–118] Pt,[119–122] Cu,[123–125] and Pd[126–129]), resonant collective oscillation of the valence electrons occurs when the frequency of the incident photons matches with the natural frequency of surface electrons that oscillate against the restoring force of the positive nuclei, thus exhibiting their characteristic plasmon absorption bands.[130] In general, the frequency of the surface plasmon absorption band strongly depends on their component, size, shape, and surrounding medium.[107,131] Au,[107] Ag,[113] Pt,[120] and Cu[125] particles exhibit the LSPR excitation in the visible light region,[132] when combined with TiO_2, they can act as photosensitizers for the excitation of TiO_2 under visible light irradiation via transferring electrons from photoexcited metals to TiO_2,[108,133] and/or supplying additional energy caused by the LSPR-induced electromagnetic fields for the photoexcitation of TiO_2.[121,122] However, the reactivity and fast oxidation of Cu under ambient conditions usually limited the study of Cu plasmons,[134] and thus most of the LSPR based TiO_2 were focused on the noble metal because of the relative chemical inertness.[107,113,130] Silva et al. reported that Au nanoparticles supported on P25 (Au/TiO_2), which exhibited a surface plasmon band with $\lambda_{max} \approx 550$ nm, can produce 0.1 mL
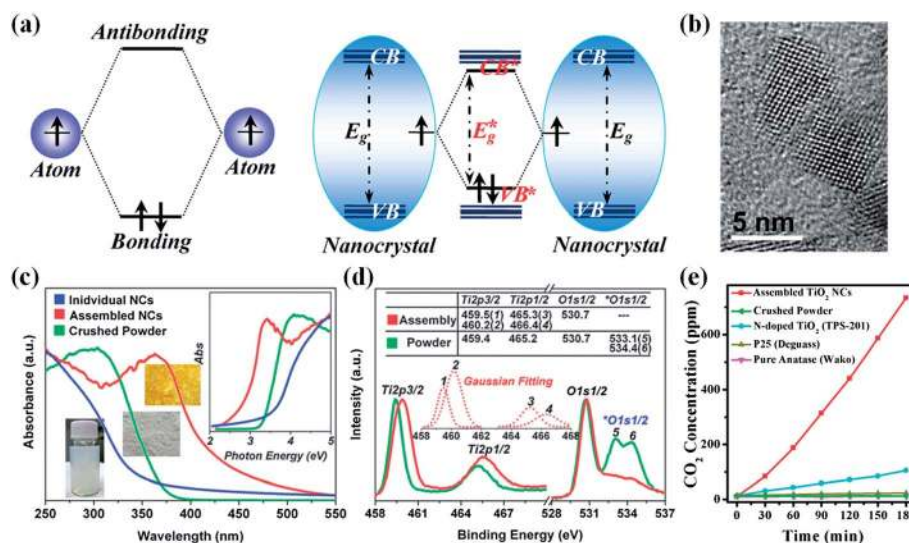

Fig. 4 (a) Illustration of the electronic bond formed between two atoms and two nanocrystals. (b) High-resolution transmission electron microscopy (HRTEM) image of individual TiO_2 nanocrystals (NCs). (c) UV-visible absorption spectra, photographs, and the converted spectra as a function of photon energy based on the Butler equation (inset) of colloidal TiO_2 nanoparticles, assembled TiO_2 NCs, and crushed NC powder. (d) Comparison of XPS spectra between assembled TiO_2 NCs and crushed NC powder. (e) Photocatalytic decomposition of IPA under visible light irradiation ($\lambda > 420$ nm). Reproduced with permission from ref. 4 (copyright 2012 Wiley-VCH Verlag Gmbh) and ref. 56.

h^{-1} H$_2$ under 532 nm laser irradiation.[135] In that work, it was assumed that the photoexcited Au injects its electrons into the conduction band of TiO$_2$ to reduce H$_2$O to H$_2$, while the holes that remain on Au quench the sacrificial electron donor to complete the entire water splitting process.[135] Zhai *et al.* revealed that Pt/TiO$_2$ films exhibited high selectivity and relatively long-term stability for selective oxidation of aromatic alcohols to aldehydes under visible light irradiation because of the LSPR effect of Pt.[122] In Zheng *et al.*'s study, plasmonic composites M@TiO$_2$ (M = Au, Ag, Pt) with LSPR excitation of the visible-light-response were systematically investigated. Au@TiO$_2$ and Ag@TiO$_2$ exhibited the LSPR peaks around 540 and 451 nm, respectively, while no obvious LSPR peak but a wide absorption band can be probed for Pt@TiO$_2$.[105,136] When evaluating their photocatalytic properties for oxidation of benzene to phenol under visible light ($\lambda > 400$ nm), Au@TiO$_2$ exhibited the highest yield in selective organic transformation.[136] However, those above-mentioned studies have mainly been limited to reactions under visible light. The question of how to achieve photocatalytic activity in the near-infrared region, which accounts for a larger proportion of solar energy, is still a big challenge.[137,138]

To achieve more visible or near-infrared light, we should tune the LSPR modes of those plamonic metals to the longer wavelength region *via* size or shape control.[105] With the increase of the particle size for a certain metal, the LSPR peak will be red-shifted due to the electromagnetic retardation in larger particles.[105] For instance, the LSPR extinction peak of Pt spheres gradually shifted from 248 to 494 nm when the diameter of Pt increased from 29 nm to 107 nm.[120] Shape control is another effective method to tune the LSPR band position. The LSPR mode of Pd nanoparticles (<10 nm in size) was reported in the UV region, however, both Pd nanoplates[126] and nanocubes[127] can exhibit the LSPR peak in the visible region; more interestingly, the LSPR locations were tuned from 410 to 520 nm when the nanocubes were cavitated into nanoboxes,[127] and the discrete dipole approximation (DDA) calculations even indicate that this location can be further red-shifted to 870 nm for the Pd nanocage with an edge length of 48 nm and a wall thickness of 3 nm.[127] In addition, in contrast to spherical Au particles, which only exhibit a transversal plasma at ∼520 nm, the plasmon resonance absorption of Au nanorods splits into two modes, which correspond to the oscillation of free electrons parallel (referred to as the longitudinal plasma) and perpendicular (referred to as the transversal plasma) to the long axis of the rods.[139] When the length-to-width ratio of the rod increases, the LSPR mode parallel to the long axis can be red-shifted to the near-infrared light region in addition to the increased oscillator strength.[105,129]

Accordingly, we carried out a study to demonstrate that the use of Au nanorods instead of spherical Au particles enables the absorption of photosensitized TiO$_2$ to be shifted to the longer visible/near-infrared region.[57] As shown in Fig. 5a, well dispersed Au nanorods (bright contrast) can be discerned in high angle annular dark field (HAADF) scanning transmission electron microscopy (STEM) images of the composite material; HRTEM images revealed that the Au nanorods and TiO$_2$ nanoparticles are in close contact with each other (Fig. 5b), which facilitates electron/energy transfer between them. Most importantly, besides the transversal plasma located at ∼520 nm, the longitudinal mode strongly depends on the aspect ratio (defined as length divided by width) of the nanorods due to the difference in charge accumulation parallel and perpendicular to the rod axis. The restoring force is proportional to this charge accumulation, and thus smaller forces and consequently smaller resonance frequencies are required to excite the longitudinal plasmon resonance. Tuning the aspect ratio of the Au nanorods allowed samples with longitudinal plasma resonances centred at 630, 660, 710, 760, and 810 nm to be prepared (Fig. 5c). The photocatalytic oxidation of IPA served as a model reaction to evaluate the wavelength dependence on the photocatalytic activity of Au-sensitized TiO$_2$ for two different types of broadband light irradiation: (I) visible light covering the transversal plasmon resonance of the Au nanorods only (400 < λ < 650 nm), and (II) visible light covering both the transversal and longitudinal plasmon resonances of the Au nanorods (400 < λ < 820 or 910 nm). As shown in Fig. 5d, both the production of acetone and CO$_2$ were much higher under broadband II irradiation than under broadband I irradiation, indicating that IPA photo-oxidation can be driven by the longitudinal plasma of Au nanorods. This greatly extends the light harvesting region from ∼520 nm for spherical Au particles to ∼810 nm for Au nanorods.[57]

3. Better charge separation

After photoexcitation, the generated electrons and holes migrate to the TiO$_2$ surface; a better charge separation efficiency is hence favourable for photocatalytic reactions. Doping can narrow the bandgap of TiO$_2$ to allow visible light harvesting. However, the undesirable charge recombination that occurs frequently at the dopant sites severely degrades the photocatalytic performance. For TiO$_2$ photoelectrodes, doping can increase the electronic conductivity and one may thus expect it to enhance the photoelectrochemical properties. Conversely, a large number of studies have revealed that the monochromatic incident photon-to-electron conversion efficiency (IPCE) decreases in the intrinsic light absorption region of TiO$_2$ after doping, because significant charge recombination occurs in the depletion region of doped TiO$_2$.[75–77] However, the latest reports in this area have demonstrated that selective doping of inner layers of the TiO$_2$ electrode can greatly enhance the photocurrent by effectively suppressing the charge recombination. In addition, particular dopants (Cr–TiO$_2$) can convert n-type TiO$_2$ into p-type. Here, the inner layer of the electrode is locally doped (p-Cr–TiO$_2$) while maintaining pure n-TiO$_2$ in the outer layer; this allows a p–n junction to be precisely formed for better charge transfer in the TiO$_2$ electrode, enabling better charge separation for photoelectrochemical solar water splitting. In powder samples, introducing disorder on the surface layers of nanophase TiO$_2$ through hydrogenation might create stable mid-gap electronic states, thus localizing both the photoexcited electrons and holes and preventing fast recombination.
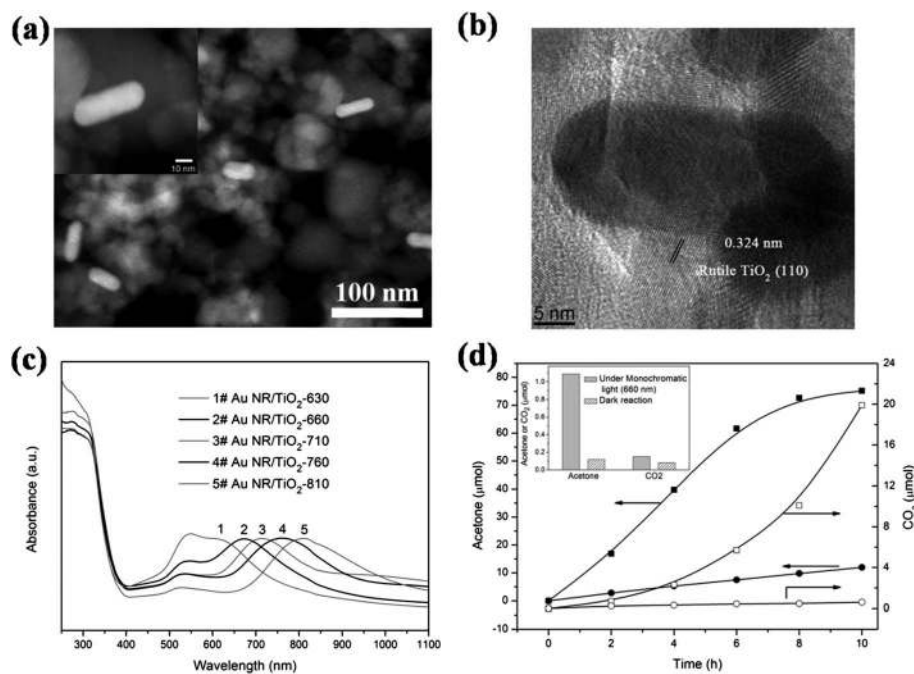
Fig. 5 (a) HAADF-STEM images and (b) HRTEM image of a Au nanorod/TiO_2 photocatalyst. (c) UV/visible absorption spectra of Au nanorod/TiO_2 photocatalysts. (d) Time dependence of acetone (solid symbols) and CO_2 (open symbols) evolution in the photocatalytic oxidation of IPA using the Au nanorod/TiO_2 photocatalyst with a longitudinal band centred at 660 nm under irradiation with broadband light I (circles) and II (squares). Reproduced with permission from ref. 57 (copyright 2013 Wiley-VCH Verlag Gmbh).

3.1 Local doping in TiO_2 photoelectrodes

When a TiO_2 electrode is immersed in aqueous solution, the energy bands close to the surface are bent (this is known as the depletion region) whereas the energy bands of the inner part remain flat (this is known as the neutral region). Accordingly, the TiO_2 electrode is divided into an "inner layer" (the neutral region) and an "outer layer" (the depletion region and the surface), as shown in Fig. 6a.[140,141] Under solar light illumination, the depletion region can absorb more light and generate more electron–hole pairs than the inner neutral region, and the electric field that exists in the depletion region can enhance the charge separation efficiency. Therefore, it is generally assumed that the depletion region (several tens of nm in thickness) contributes most of the available electrons and holes for photocatalytic reactions.[142] To date, most studies have been performed on uniformly doped TiO_2 electrodes, in which the dopants were homogeneously distributed over both the neutral and depletion region of TiO_2. Doping can increase the carrier density directly and thus result in a narrower depletion region,[143,144] which greatly degrades the electron–hole separation ability and causes electron–hole recombination at the dopant sites, accompanied by decreased IPCE.[71,145]

To solve these problems, considering that doping in the outer layer has a negative effect on the electron–hole separation, we selectively doped nitrogen (N) on the inner layer of a TiO_2 film using pulsed laser deposition (PLD) in a N_2 atmosphere.[76] As presented in Fig. 6b, the energy dispersive X-ray spectroscopy (EDS) spectra of the TiO_2 electrode (total thickness ∼200 nm) revealed that N was selectively doped in the inner layer of the

TiO_2 film (thickness ∼120 nm), and that N was absent in the outer region of the film (∼80 nm). For such inner-doped TiO_2 electrodes, N-doping can improve both the carrier density and electronic conductivity in the neutral region, whereas a wide depletion region is maintained in the outer non-doped layer. In this case, the inner N-doped TiO_2 electrode exhibited an excellent photocurrent density (400 μA cm^{-2} at 1.23 V vs. standard hydrogen electrode (SHE) under 100 mW cm^{-2} solar simulator illumination), much higher than those of pure TiO_2, outer N-doped TiO_2, and uniformly N-doped TiO_2 electrodes (Fig. 6c). An IPCE measurement further confirmed that the inner N-doped TiO_2 electrode exhibited a much higher IPCE than that of pure TiO_2, outer and uniformly N-doped TiO_2 electrodes in the light region with λ < 400 nm. Under monochromatic light irradiation (centred at 320 nm), an IPCE of as much as 95% was achieved for the inner N-doped TiO_2 electrode (Fig. 6d). This study suggests that the effects of doping in different regions of TiO_2 electrodes should be analysed more carefully in practical photoelectrochemical tests.[76]

In contrast to pure and N-doped TiO_2, which are n-type semiconductors and hence only suitable as the anodes for oxidization reactions, Cr-doped TiO_2 is a p-type semiconductor and was fabricated as a cathode for photo-reduction in our group.[77] We fabricated Cr-doped TiO_2 thin films at a relatively low substrate temperature of 550 °C by PLD.[77] Two peaks observed in the XPS spectra at 586.1 eV and 576.3 eV were assigned to the $2p_{1/2}$ and $2p_{3/2}$ binding energies of Cr ions, respectively (Fig. 7a); the O 1s peak was observed at 529.3 eV (inset of Fig. 7a). These spectra confirmed that the TiO_2 films were doped with Cr^{4+}. The

This journal is © The Royal Society of Chemistry 2014

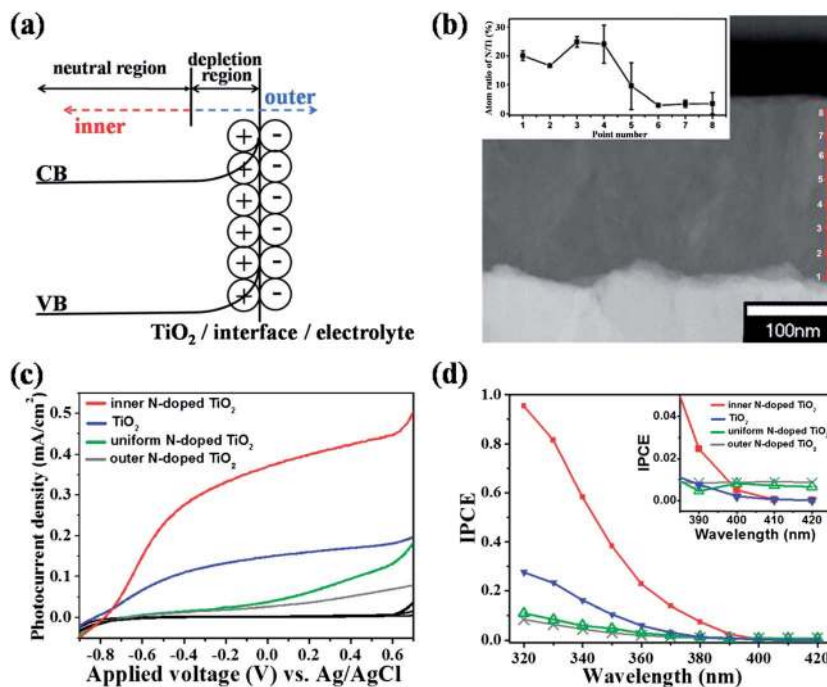J. Mater. Chem. A, 2014, 2, 12642–12661 | 12649

Fig. 6 (a) Band structure of a TiO_2 photoelectrode interacting with the electrolyte. (b) STEM image (dark field) and atomic ratio of N/Ti at different locations (inset) of the inner layer of a N-doped TiO_2 thin film. (c) I–V curves and (d) IPCEs of pure TiO_2, uniformly N-doped TiO_2, outer-layer N-doped TiO_2, and inner-layer N-doped TiO_2 electrodes. Reproduced from ref. 76.

photocathodic I–V curves indicated that Cr-doped TiO_2 is a p-type semiconductor (Fig. 7b). More significantly, by selectively doping Cr in the inner layer of the TiO_2 film, the photocurrent density was increased to a relatively high value of -69.4 μA cm^{-2}, much larger than in uniformly Cr-doped TiO_2 (-13.2 μA

cm^{-2}) at -0.4 V vs. Ag/AgCl. In contrast to the single depletion region that exists in uniformly Cr-doped TiO_2 electrodes (Fig. 7c), two depletion regions (depletion region I at the p-type Cr-doped TiO_2–n-type TiO_2 interface and depletion region II at the n-type TiO_2–electrolyte interface) were observed for the
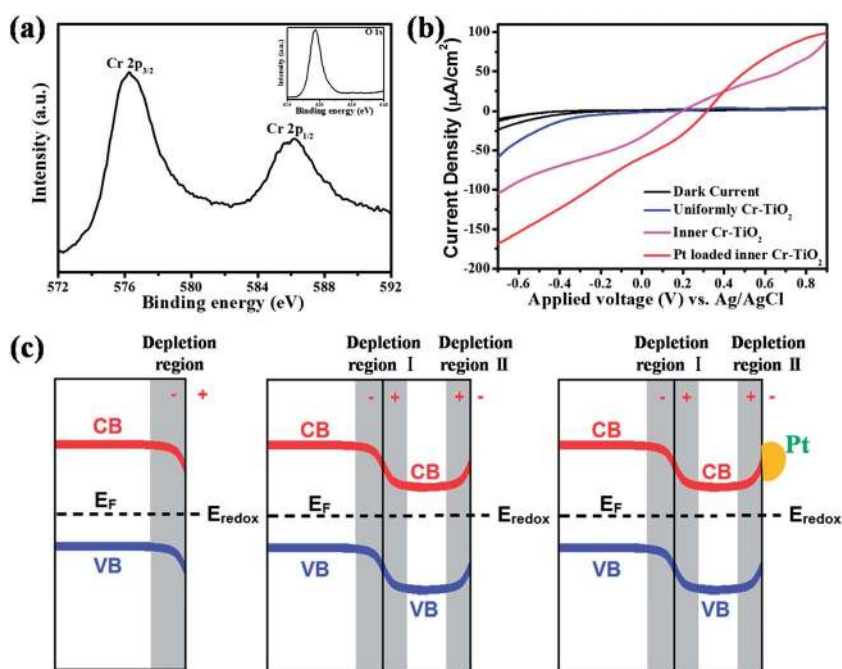

Fig. 7 (a) XPS spectrum showing Cr 2p and O 1s (inset) peaks for uniformly Cr-doped TiO_2. (b) I–V curves of the as-prepared Cr-doped TiO_2 thin films. (c) Band structures of films of uniformly Cr-doped TiO_2 (left), inner Cr-doped TiO_2 (center), and inner Cr-doped TiO_2 with Pt loading. Reproduced from ref. 77.

inner Cr-doped TiO_2 photoelectrode. Depletion region I can drive the transfer of electrons to the electrode surface, which has a positive effect on the p-cathode; however, the presence of depletion region II might hinder this electron transfer. To overcome this negative effect, we deposited Pt nanoparticles on the surface of the TiO_2 electrode in order to construct a TiO_2/Pt interface instead of the TiO_2/electrolyte interface (Fig. 7c). Electrons can move to the Pt nanoparticles more easily because they do not have to overcome the high barrier associated with the TiO_2/electrolyte interface. After Pt loading, both the photocurrent density and the onset potential were significantly enhanced (Fig. 7b).[77]

3.2 Surface disorder in TiO_2 powders

An alternative approach to conventional impurity doping, which generates discrete donor or acceptor states near the conduction band or valence band edge of a semiconductor, is the introduction of a large degree of lattice disorder, which might yield stable mid-gap states. Such mid-gap states (also known as band-tail states) can form a continuum extending to and overlapping with the conduction/valence band edge (Fig. 8a). This can not only narrow the bandgap of TiO_2 but also localize the photoexcited charge carriers and prevent fast charge recombination.[20,146–149]

Recently, Chen et al. reported that introducing disorder on the surface layer of nanophase TiO_2 through hydrogenation (resulting in a sample referred to as "black TiO_2") can create stable mid-gap states close to the valence band of TiO_2.[20] Experimentally, TiO_2 nanocrystals were hydrogenated in a 20.0 bar H_2 atmosphere at 200 °C for 5 days to obtain the surface-disordered TiO_2 sample. HRTEM images showed that the pure TiO_2 nanocrystals were highly crystalline (Fig. 8b), whereas after hydrogenation, a crystalline core and a highly disordered surface layer (~1 nm in thickness) could be distinguished when

the hydrogen dopant was introduced (Fig. 8c). The onset of optical absorption was drastically shifted from the UV region to the near-infrared (~1200 nm) after hydrogenation (Fig. 8d), accompanied by a colour change from white to black (inset of Fig. 8d). The abrupt change in the absorbance spectra that occurred at ~800 nm suggests that the bandgap of black TiO_2 was substantially narrowed by intraband transitions.[20] Valence band XPS spectra (Fig. 8e) showed that in comparison with the white TiO_2 sample, for which the valence band edge was at 1.26 eV, black TiO_2 exhibited a valence band edge that was shifted towards the vacuum level at −0.92 eV, which accounts for the onset of optical absorption at ~1200 nm. Calculations based on first-principles density functional theory (DFT) confirmed that the disorder-induced mid-gap states formed by hybridization of the O 2p orbitals and Ti 3d orbitals can indeed up-shift the valence band edge of TiO_2 (Fig. 8f); the hydrogen dopant stabilizes the lattice disorder by passivating dangling bonds on the surface. Most importantly, because the mid-gap states are derived from the hybridization of O 2p and Ti 3d orbitals, an optical transition between these mid-gap states and the conduction band tail would produce charge transfer from O 2p states to Ti 3d states, similar to the transition from the valence band to the conduction band in bulk TiO_2. This localization of both photoexcited electrons and holes can prevent the occurrence of fast recombination, which overcomes the drawback that dopants usually act as charge recombination centres in photocatalytic reactions. In photocatalytic H_2 evolution, black TiO_2 produced ~0.1 mmol h^{-1} g^{-1} H_2 under visible/infrared light irradiation, indicating that the mid-gap states resulting from surface disorder indeed narrow the bandgap of TiO_2.[20] This disorder engineering not only enables visible/infrared light harvesting, but also improves the charge separation in photocatalytic reactions, and thus can be considered as a feasible strategy for both environmental and energy applications.
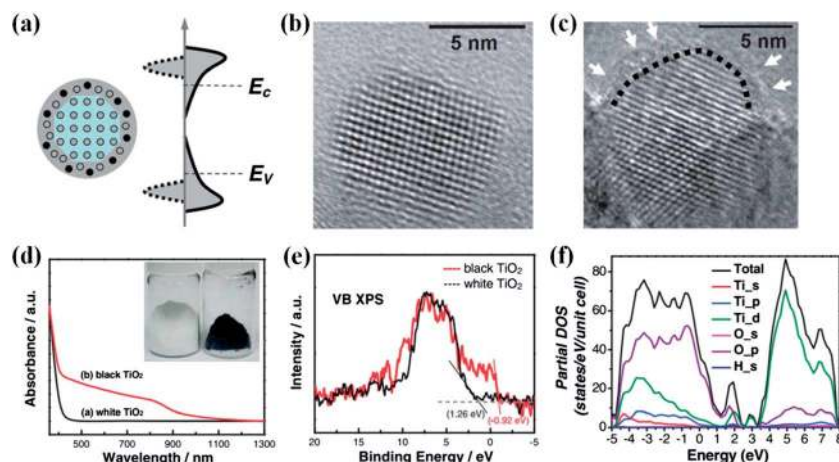

Fig. 8 (a) Schematic illustration of the structure and electronic density of states (DOS) of a semiconductor nanocrystal with surface disorder. (b) HRTEM image of the TiO_2 nanocrystal. (c) HRTEM image of the TiO_2 nanocrystal after hydrogenation (the interface between the crystalline core and the disordered outer layer is outlined by the dashed curve). (d) Absorption spectra and photographs (inset) of the TiO_2 nanocrystals before and after hydrogenation. (e) Valence–band XPS spectra of the white and black TiO_2 nanocrystals. (f) Decomposition of the total DOS of surface-disordered black TiO_2 nanocrystals into partial DOS of the Ti, O, and H orbitals. Reproduced with permission from ref. 20 (copyright 2011 American Association for the Advancement of Science).

4. Optimized surface reactivity

Because photocatalytic redox reactions take place on the surface, the surface reactivity of TiO_2 has a strong influence on the photocatalytic activity.[78] To determine the surface reactivity, not only the surface atomic structure (the density of under-coordinated Ti atoms), but also the surface electronic structure (the redox potential of the photoexcited charge carriers) should be considered. Furthermore, special attention should be paid on the distribution of charge carriers (e^-–h^+) on the specified facet, which will affect the charge separation efficiency.

4.1 Surface chemistry of TiO_2 single crystals

It is of great importance to study the surface chemistry of TiO_2. In general, surfaces with high surface energy disappear rapidly during the crystal growth process in order to minimize the total surface energy. According to the Wulff construction and the calculated surface energy, under equilibrium conditions anatase TiO_2 adopts a slightly truncated tetragonal bipyramidal shape with 94% of the surface area accounted for by {101} surfaces and the remainder by {001} surfaces (Fig. 9a-I); no {100} surfaces will appear despite its calculated surface energy (0.53 J m^{-2}) lying between those of the {101} (0.44 J m^{-2}) and {001} surfaces (0.90 J m^{-2}).[78]

Nevertheless, the introduction of appropriate surface adsorbates can substantially lower the energy of the anatase {001} surface and selectively control the growth rates of related crystal planes.[78] Yang et al. calculated the energies of each surface when terminated with 12 different non-metallic atoms;[17] it was revealed that fluorine (F) termination can most effectively lower the energies of both the {001} and {101} surfaces, leading to crystals with dominant {001} surfaces. Experimental results subsequently verified this theoretical predication; anatase TiO_2 single crystals with 47% active {001} facets were grown using HF as a crystallographic controlling reagent.[19] This significant finding indicates that the selective adsorption of ions on high-energy surfaces can induce TiO_2 crystals to grow preferentially along a desired crystallographic direction.[150–152] To date, TiO_2 nanosheets comprising nearly 100% exposed {001} facets have been experimentally realized by dissolving diethylenetriamine in isopropyl alcohol as a capping reagent.[84] In addition to the {001} surface,[153,154] {100} facets have also been confirmed to exist as the "belt" in the centre of TiO_2 particles (Fig. 9a-II); the preferential adsorption of hydroxyl ions on the {100} surface can stabilize it, leading to TiO_2 with a higher percentage of exposed {100} facets.[155,156] Experimentally, TiO_2 nanorods exposed with a large percentage of {100} facets were reported to be synthesized by hydrothermal transformation of either alkali titanate nanotubes in basic solution[157] or $H_{0.68}Ti_{1.83}O_4$ particles in aqueous solution.[158] TiO_2 nanocuboids with dominant {100} facets were also solvothermally prepared via carboxymethyl cellulose,[159] or acid-delaminated vermiculite and tetramethylammonium hydroxide,[160] or the ionic liquid 1-butyl-3-methylimidazolium tetrafluoroborate[81] as the capping agents.

4.2 Surface reactivity in photocatalytic reactions

For anatase TiO_2, the most extensively investigated surfaces are {101}, {001} and {100}. In contrast to the {101} surface, for which only 50% of the Ti atoms are five-coordinated (Ti_{5c}), both the {001} and {100} surfaces consist of 100% Ti_{5c} atoms (Fig. 9b).[78] The Ti_{5c} atoms can act as active sites in the photocatalytic process.[85] Therefore, from the viewpoint of the surface atomic structure, the {100} and {001} facets should be more active than the {101} facet. Han et al. systematically controlled the shape of TiO_2 single crystals from a tetragonal bipyramidal shape enclosed by {101} facets to a truncated tetragonal bipyramidal bounded with a combination of {001} facets and {101} facets, to sixteen-faceted polyhedral exposed to {103} and {101} facets, and then to pudgy tetragonal bipyramidal enclosed by {102} facets. The photooxidation of methylene blue (MB) was further carried out to evaluate the surface-dependent photocatalytic properties of those TiO_2 nanocrystals which are in the order of truncated tetragonal bipyramidal > pudgy tetragonal bipyraidal > sixteen-faceted polyhedral > tetragonal bipyramidal, and the higher activity is related to the percentage of active facets exposed. It is reported that the {001} facet has a high surface energy, and both the high density of surface undercoordinated Ti atoms and the presence of enlarged Ti–O–Ti bond angles at the surface make the Ti and O atoms very reactive, thus facilitating the photodegradation of MB.[161–164] Since the truncated tetragonal bipyramidal composed of a 45% {001} facet, it exhibited the highest photocatalytic activity; while the tetragonal bipyramidal dominantly surrounded with the most stable {101} facets, which showed the lowest activity. Both {102} and {103} surfaces have a similar structure which were consisted of units of {001} subfacets, thus should exhibit similar activity but higher than the {101} surface; however, besides the {103} facet, the sixteen-faceted polyhedral also exposed with eight {101} facets, leading to a lower activity than that of pudgy tetragonal bipyramidal with major {102} facets exposed. Accordingly, the order of photooxidation efficiencies for various surfaces was deduced to be {001} > {102} ≈ {103} > {101}.[165]

Nevertheless, when operating the photocatalytic tests in H_2 evolution from H_2O, a contradictory reaction order ({100} > {101} > {001}) was revealed for the anatase TiO_2 samples with dominant {101}, {001}, and {100} facets.[80] It is pointed out the different atomic coordination and arrangement on each surface (Fig. 9b) will give rise to different surface electronic configurations, and thus the electronic band structure of TiO_2 will depend on which facets are exposed.[85,158] In Pan et al.'s study, the conduction band minimum of TiO_2 is in the order of {100} > {101} > {001}, and thus more reductive electrons can be produced on TiO_2 exposed with more {100} and {101} facets to reduce H_2O into H_2, followed with a higher photocatalytic activity. Despite that the {001} facet has a higher surface energy and 100% of Ti_{5c} on its surface, the poor electronic band structure really hinders the H_2 production efficiency.[80] Therefore, even the Ti_{5c} atoms can act as active sites to facilitate the reactant adsorption on both {100} and {001} surfaces, and the superior surface electronic structure of the {100} facet makes it more reactive in the photoreduction test because of the more reductive electrons generated.
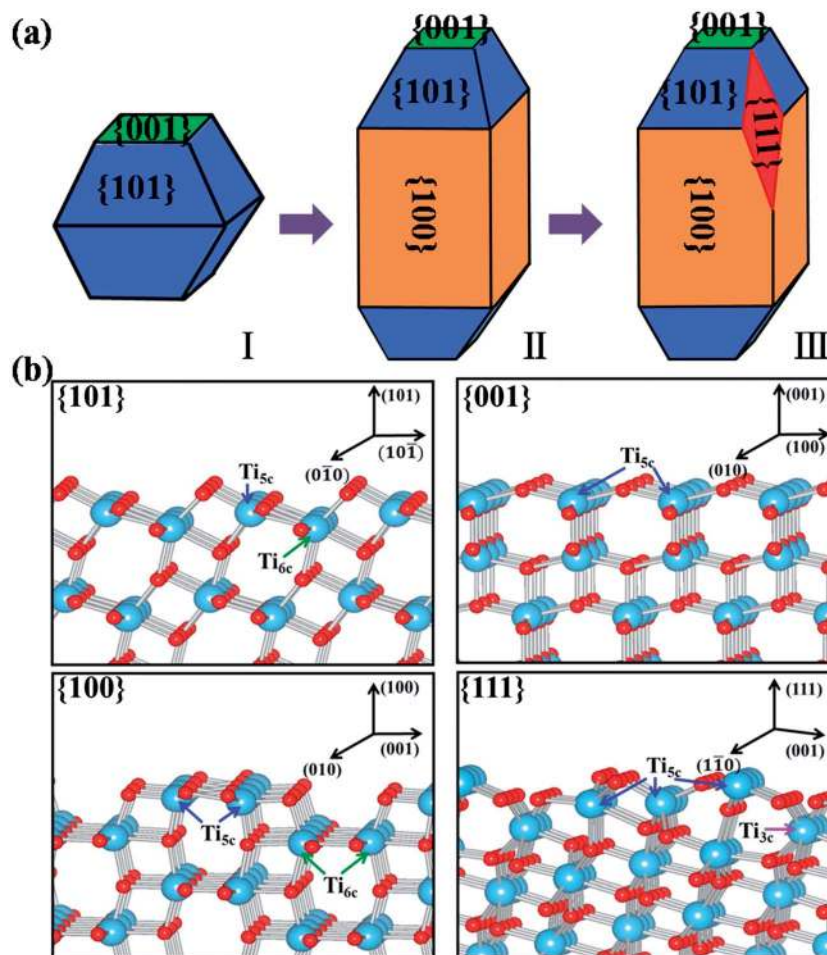
12652 | *J. Mater. Chem. A*, 2014, **2**, 12642–12661

This journal is © The Royal Society of Chemistry 2014

Fig. 9   (a) Schematic pictures of anatase TiO_2 crystals with various surfaces exposed. (b) Structures of relaxed stoichiometric {101}, {001}, {100}, and {111} surfaces. Reproduced with permission from ref. 85 (copyright 2012 American Chemical Society).

Compared to the above results for the {100} facet, we have recently found that the {111} facet (Fig. 9a-III) exhibits superior properties with respect to both the surface atomic structure and electronic structure.[85] DFT calculations predict that the surface energy of the {111} facet is 1.61 J m^{-2}, which is partially attributed to the large percentage of under-coordinated Ti atoms ($Ti_{5c} : Ti_{3c} = 3 : 1$) and the presence of O atoms (100% O_{2c}) on the surface (Fig. 9b). To overcome this high surface energy experimentally, both fluorine and ammonia were used as capping reagents to stabilize the {111} facet. Electron diffraction (SAED) showed that the resulting square TiO_2 nanoplates were single crystals (Fig. 10a); the zone axis was indexed to [111]. HRTEM images revealed that the interfacial angle between the (101) and (011) atomic planes of anatase TiO_2 is 82° (Fig. 10b), further confirming that the exposed crystal plane is the {111} facet. The numerous under-coordinated O atoms (100% O_{2c}) on the {111} facet facilitate the formation of oxygen vacancies, which can act as active sites in photocatalytic reactions. The electron spin resonance (EPR) signal at $g = 2.002$ (Fig. 10c) indicated the presence of Ti^{3+} on the surface; in comparison to TiO_2 samples in which the other three facets were dominant, the intensity of the signal in the T111 sample was much

stronger, implying the presence of more oxygen vacancies on the T111 surface.[166,167] Furthermore, the UV-visible absorption spectra (Fig. 10d) and valence band XPS spectra showed that TiO_2 with exposed {111} facets possesses a superior electronic band structure to that of the previously discussed T100 sample (Fig. 10e). Tests of the photocatalytic activity in water splitting showed that TiO_2 with {111} facets exposed yielded H_2 evolution in quantities ~5 times greater than for TiO_2 with {100} facets exposed (Fig. 10f). This excellent photocatalytic efficiency can be ascribed to the optimized surface atomic structure and electronic band structure.

4.3   Charge separation between {001} and {101} facets of TiO_2

As aforementioned, the surface reactivity is in the order of {001} > {101} in photooxidation of MB because of its higher surface energy and 100% of Ti_{5c}, while {101} is superior to {001} in H_2 production related to its higher conduction band minimum. The former is emphasized to offer active sites on the TiO_2 surface, and the latter is focused on the more reductive electrons produced. Moreover, the charge migration process from bulk to surface is also need to be considered in the facet-
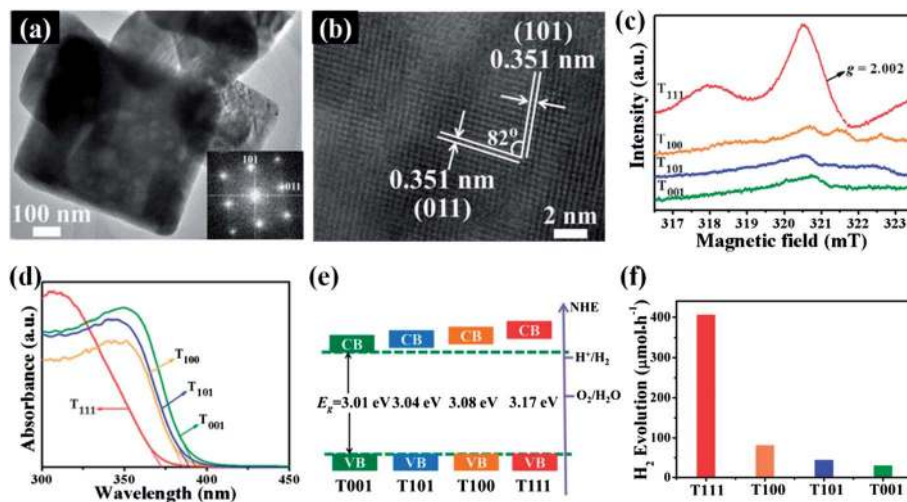
This journal is © The Royal Society of Chemistry 2014

J. Mater. Chem. A, 2014, 2, 12642–12661 | 12653

Fig. 10 (a) TEM image of TiO$_2$ with {111} facets exposed, and the corresponding SAED pattern (inset). (b) HRTEM image of this TiO$_2$ sample. (c) EPR spectra of TiO$_2$ with various facets exposed. (d) UV–visible absorption spectra of the TiO$_2$ samples. (e) Schematic band structures of TiO$_2$ with various facets exposed. (f) Photocatalytic water splitting tests on Pt-loaded (0.5%) TiO$_2$ samples with various facets exposed under UV–visible light irradiation ($\lambda > 300$ nm). TiO$_2$ with dominant {111}, {100}, {101}, and {001} facets are denoted as T111, T100, T101, and T001, respectively. Reproduced with permission from ref. 85 (copyright 2012 American Chemical Society).

engineered TiO$_2$ single crystal. *Via* detecting the deposition sites of noble metals (Au, Ag, and Pt) or metal oxides (PbO$_2$ and MnO$_x$), we can primarily justify whether the crystal facet is for reductive sites or oxidation sites; therefore, TiO$_2$ single crystals exposed with various facets can effectively reinforce the photo-generated e$^-$ and h$^+$ to be distributed in different facets, thus realizing the charge separation.[168,169] Ohno *et al.* found that more PbO$_2$ particles which were oxidized from Pb^{2+} *via* h$^+$ were deposited on rutile {011} and anatase {001} facets than that on rutile {110} and anatase {101} facets, indicating that the pho-togenerated h$^+$ are mainly accumulated on rutile {011} and anatase {001} facets acted as oxidation sites while e$^-$ are mostly distributed on rutile {110} and anatase {101} facets acted as reduction sites.[169] This behavior was attributed to the different energy levels of the conduction and valence bands resulting in various facets with different atomic arrangement characteris-tics; the difference in the energy levels drives the e$^-$ and h$^+$ to various crystal facets, aiming to reach the most stable energy configuration and leading to a charge separation.[170–172]

In D'Arienzo's study, to evaluate the role of the exposed crystal facet in phenol mineralization by using O$_2$ as the oxidizing agent, EPR was adopted to quantitatively monitor the formation and the interfacial reactivity of the charge-trapping sites over shape-controlled anatase TiO$_2$ nanocrystals *via* detection of the charge-trapping centers, Ti^{3+}, O$^-$, and O^{2-}, *etc.* Under vacuum conditions, the concentration of trapped h$^+$ (O$^-$ center) increased with a higher {001} surface area, followed by a higher photoactivity; whereas the amount of Ti^{3+} centers (caused by the reduction of Ti^{4+} *via* e$^-$) increased with more {101} facet exposed, but with a weaker photooxidative activity. Those results suggested that the {001} surface is for oxidation sites with a key role in photooxidation while {101} surfaces provide reductive sites which do not directly assist the oxidative process. Furthermore, photoexcitation experiments in an O$_2$

atmosphere led to the formation of Ti^{4+}–O$_2^-$ oxidant species mainly located on {101} facets, confirming the indirect contri-bution of {101} surfaces to the photooxidative process.[173]

Therefore, we can conclude that the specific exposed facets also influence the charge trapping and interfacial transfer process of the photogenerated e$^-$–h$^+$, in which the {001} facet prefers oxidation while {101} favours the reduction.

5. Theoretical studies

Theoretical studies, particularly electronic structure calcula-tions and molecular dynamics simulations, have been exten-sively performed to gain insight into the photocatalysis phenomenon. In general, a photocatalytic reaction consists of three steps: photoexcitation to generate electrons and holes, charge transfer from the bulk to the surface, and redox reaction on the surface. Accordingly, theoretical studies address each of these three steps.[4]

Doping is the most popular way to tailor the absorption edge of TiO$_2$. However, doping is usually accompanied by defects in the TiO$_2$ matrix, which can act as carrier recombination centres with a negative effect on the charge transfer process. Therefore, to obtain better light absorption while avoiding undesirable recombination, more systematic theoretical studies are neces-sary to better understand the effects of doping. In calculations, doped materials are usually described by introducing a foreign element into a sufficiently large extended unit cell (supercell) with geometric relaxation performed using DFT. Asahi *et al.* have studied the effects of anion doping in anatase TiO$_2$ by means of DFT calculations within the local-density approxi-mation, and suggested that nitrogen is the most promising dopant for an upward shift of the valence band maximum, thus enhancing visible-light absorption.[17] Although this computa-tional result was consistent with experimental findings by the

12654 | *J. Mater. Chem. A*, 2014, **2**, 12642–12661

This journal is © The Royal Society of Chemistry 2014

same authors that nitrogen doping induces a red-shift of the absorption edge, their interpretation based on a small supercell containing 6 atomic % of nitrogen has been questioned by subsequent work.[174–176] Actual TiO_2 samples can accommodate no more than 1% nitrogen,[17,177,178] and the electronic structure of samples with this much lower concentration of nitrogen is significantly different from that described in ref. 17; a substitutional N atom at an O site (N_O) creates an occupied state far above the valence band maximum (a deep impurity state) rather than a hybrid band consisting of N 2p states and the host valence band.[174–176] Such deep impurity states can act as carrier recombination sites[179] and possibly degrade the carrier transfer process. Therefore, substitutional nitrogen alone cannot explain the oxidation reaction that was experimentally observed on N-doped TiO_2.

Recently, Umezawa et al. reported a comprehensive theoretical analysis of N-doped TiO_2, which not only revealed the origin of the visible-light absorption but also gave a reasonable explanation of the photocatalytic oxidation reactions facilitated by N-doped TiO_2.[180] Using DFT incorporating onsite Coulomb interactions (DFT + U), it was suggested that a N_O prefers to bond with Ti atoms at interstitial sites (Ti_i) to form complex defects, N_O–Ti_i. This promotes the hybridization of N p states with the Ti d states of Ti_i, giving rise to broader energy states at the valence band edge and eliminating the hole trapping centres associated with the deep N_O states. Fig. 11a and b show band structures for the up-spin states of a negatively charged N_O^{-1} and a neutral $[N_O–Ti_i]^0$, respectively. The deep impurity states associated with a N_O^{-1} are replaced by multiple states above the valence band of the host TiO_2 for the complex $[N_O–Ti_i]^0$ defects (Fig. 11b) due to the formation of bonding and anti-bonding states.[180] The DOS plot in Fig. 11d shows that the defect–impurity hybrid states associated with $[N_O–Ti_i]^0$ are connected under an appropriate smearing parameter (0.1 eV) representing thermal fluctuation. By contrast, the deep

impurity state associated with N_O^{-1} remains disconnected from the valence band maximum of the host material (Fig. 11c), which is consistent with previous reports.[174–176] The calculated bandgap (2.4 eV) for $[N_O–Ti_i]^0$ is in good agreement with experimental data.[177,178] This scenario is further supported by the migration properties of Ti_i shown in Fig. 11e. The second barrier in the migration path of Ti_i^{+1} disappears when it migrates towards N_O^{-1}, and the total energy monotonically decreases along the migration path until the complex $[N_O–Ti_i]^0$ is formed. The estimated migration barrier is ~0.7 eV, which is readily overcome at a typical annealing temperature of 550 °C. This study offers a reasonable explanation for the good, visible-light-driven photo-oxidation ability of N-doped TiO_2.[180]

The separation of electron–hole pairs is an important factor to control in order to enhance photocatalytic activity. Platinum particles on the surface of TiO_2 as a co-catalyst are beneficial for two reasons: facilitating carrier separation and lowering reaction barriers. However, the detailed mechanism of the effects of Pt as a co-catalyst has until recently been insufficiently understood. To tackle this issue from a theoretical point of view, the photo-excited carriers that are transported to a Pt/TiO_2 interface must be taken into account. Recently, Boonchun et al. have suggested a useful model involving substitutional fluorine at an oxygen site in order to better describe photo-excited electrons.[181] Fig. 12a shows the DOS for pristine anatase TiO_2 and F-doped TiO_2, which indicates that the substitutional fluorine acts as a donor and shifts the highest occupied state upto the bottom of the conduction band. In this study, the extra electron introduced by substitutional fluorine was utilized to mimic a photo-excited electron. From the partial charge densities associated with the interfacial states at Pt/TiO_2 and Pt/F-doped TiO_2 (Fig. 12b), it was found that the extra electron is mainly located at oxygen sites near the interface. This implies that the gap states induced by loading Pt on TiO_2 make energy states available for electrons to occupy; this is the likely driving force behind the electron
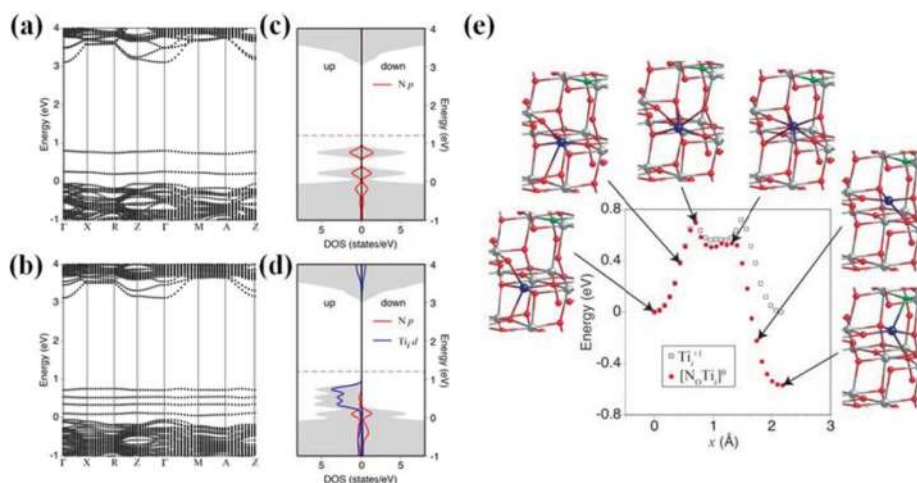

Fig. 11 Band structures of the up-spin states for (a) N_O^{-1} and (b) $[N_O–Ti_i]^0$ between highly symmetric points in the Brillouin zone associated with a 96-atom supercell. Total and local DOS for the up- and down-spin states are shown for (c) N_O^{-1} and (d) $[N_O–Ti_i]^0$. Here, the local DOS for Ti_i was integrated over the two nearest-neighbour Ti atoms. The horizontal dashed line indicates the highest occupied state. (e) Images of the intermediate configurations formed when Ti_i^{+1} migrates towards N_O^{-1} and the calculated total energy along this migration path in comparison to the total energy in the absence of N_O^{-1}. Reproduced from ref. 180.

This journal is © The Royal Society of Chemistry 2014

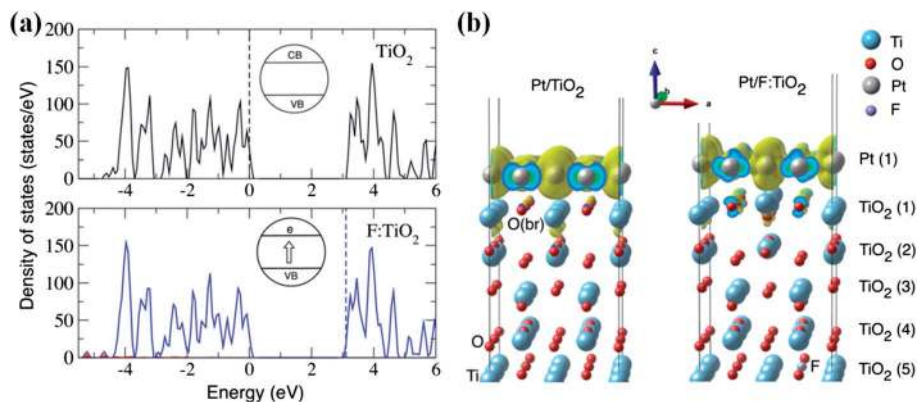J. Mater. Chem. A, 2014, **2**, 12642–12661 | **12655**

Fig. 12 (a) Perdew−Burke−Ernzerhof (PBE) calculated total DOS for bulk TiO_2 and F-doped TiO_2 at the X point in the Brillouin zone. The vertical dashed lines indicate the highest occupied state. The red shaded area indicates the F p states. (b) Partial charge density of electrons associated with metal-induced gap states at the Pt/TiO_2 interface for undoped and F-doped TiO_2. The isosurface of the density is displayed at a value of ∼0.08 electrons per $Å^3$. Reproduced from ref. 181.

transfer from the bulk TiO_2 to the Pt/TiO_2 interface. The accumulation of electrons at the Pt/TiO_2 interface leads to an upward shift of the Fermi level of the system, which allows protons (H^+) to be more readily attracted and the adsorption of H_2 on the Pt surface to be weakened.[181] Therefore, this simple model successfully explains the photocatalytic evolution of H_2 from water splitting on the surface of Pt-loaded TiO_2.

Theoretical studies have mainly focused on explanations of observed phenomena or have suggested model mechanisms. In recent years, however, there has been great demand for theory-guided prediction of better materials in order to alleviate the burden of experimental trial and error approaches. Reunchan *et al.* have succeeded in developing a theoretical design for visible-light driven photocatalysts using a co-doping scheme applied to strontium titanate.[182] The same approach is also valid for TiO_2 and it is expected that the photocatalytic performance of transition metal-doped TiO_2 can be controlled by co-doping with either donors or acceptors, or by any other method that adjusts the Fermi level of the system. A greater challenge for theoretical studies is to predict entirely novel materials with high photocatalytic activity instead of simply improving known photocatalysts. Such computational materials design can be realized only by close collaborations with experimentalists and through iterative prediction and validation procedures, and will become a key technology for accelerating the development of advanced photocatalysts.

6.   Conclusion and perspectives

In this article, we have selectively discussed recent advances in TiO_2-based photocatalysis from three of the most important aspects dominating a photocatalytic reaction: light absorption, charge separation, and surface reactivity. Starting from the strategies in enhancing light absorption, novel approaches were introduced, which were proved to be effective for increasing light absorption of TiO_2 not only from the range of wavelength, but also from the amount of light. Adopting Mie's scattering over size-optimized TiO_2 spheres is shown to be promising to

improve the intrinsic light absorption of TiO_2; to extend the light harvesting from UV to visible light region, electronic coupling emerged in the assembly of TiO_2 nanocrystals can effectively narrow the bandgap of TiO_2 and enlarge its light response to 500 nm; most significantly, the LSPR based Au nanorod photosensitization over TiO_2 can even harvest the near-infrared light. Noticeably, doping with a different element in the matrix of TiO_2 can vary the chemical composition of TiO_2 to narrow its bandgap for more visible light harvesting. However, the unexpected charge recombination occurred in the dopant center largely impede the charge transfer from bulk to surface. Then, for better charge migration, selective doping in the inner layer or modulation of the dopant for the p–n junction in TiO_2 electrodes were confirmed to be valid routes for the higher charge separation efficiency; in parallel, introducing surface disorder in hydrogenated TiO_2 powders can build stable mid-gaps in TiO_2 to localize the photogenerated charge carriers from fast recombination. Furthermore, to promote the surface reactivity, superior surface atomic and electronic structures of TiO_2 single crystals can be optimized *via* facet engineering. Finally, the latest theoretical studies were also discussed for better understanding about TiO_2-based photocatalysis, including a bold approach in understanding detailed behavior of photo-excited electrons in TiO_2 loaded with a Pt co-catalyst. With significant fundamental understanding achieved from the past research, we can believe that TiO_2-based photocatalysis represents a promising way in both environmental remediation and energy conversion. However, from the aspects of practical application, many challenges remain in the materials engineering.

It is essential to further enhance both the light absorption and charge separation *via* fabrication of TiO_2-based composite materials. Doping and solid-solution strategies can modulate the bandgap,[6,106,183,184] even though the visible-light-response can be achieved, the charge recombination occurring in the dopant center remains hard to conquer. For the practical application on a large scale, *via* combining the semiconductor with a narrower bandgap, the light absorption edge can be red-

12656 | *J. Mater. Chem. A*, 2014, **2**, 12642–12661

This journal is © The Royal Society of Chemistry 2014

shifted to a longer wavelength region for more light-harvesting; in addition, the charge transfer and accumulation process between the band-structure-matched phases will facilitate the multiple-electron reactions (*e.g.* CO_2 photoreduction), which offers a promising route for higher solar-energy conversion efficiency.[185–188]

With regard to the co-catalyst, there are indeed few details understood until now. Nevertheless, the significant influence of co-catalysts on photocatalytic activity has been known for decades,[49] and recently, the efforts in not only understanding the mechanism of the co-catalysts, but also in exploring new co-catalysts, including bimetallic alloy co-catalysts have been performed widely.[189,190] *Via* optimizing the element in alloys, the Schottky barrier between the alloy and TiO_2 can be tuned to further inhibit charge recombination.[191,192] Then more electrons can be accumulated on alloy co-catalysts for an effective CO_2 photoreduction, especially in which the resultant products largely depend on the specific reaction pathway and the number of electrons transferred, thus the product selectivity can be achieved *via* tuning the component of an alloy co-catalyst.[12] On the other hand, since different metals possess different overpotentials and adsorption abilities, we can selectively control the electron accumulation and reactant adsorption/dissociation occurring in various components of alloys to inhibit the resultant material to be further decomposed for higher productivity.[193,194] Therefore, more attention should be paid to the engineering of bimetallic alloy co-catalysts on the TiO_2 surface in the perspective research. Besides the metal co-catalyst, particular attention should also be paid on the carbonaceous nanomaterials (such as graphene,[195–197] carbon nanotubes,[198] C_{60},[199] *etc.*), which can act as electron acceptors for efficient charge separation in the photocatalytic reaction and play the role of a co-catalyst but with much cheaper cost.[200]

In addition to all the strategies described in this article, we definitely need to pay more attention on how to activate the targeting reactants (IPA, H_2O, CO_2, *etc.*) from both experimental and theoretical approaches, including development of sophisticated surface-interface engineering for realizing a higher activity. Generally, *via* forming the chemical bonding with TiO_2 not only the physically adsorption on the TiO_2 surface, but also the reactant molecules can be effectively activated with higher reactivity, and then the photocatalytic reaction can be completed with much lower chemical potential. It is known that the linear CO_2 molecule is highly stable, thus it is a big challenge to activate it in CO_2 photoreduction. Nevertheless, when chemisorbed on the basic oxides (such as MgO), CO_2 will become destabilized carbonate which is more easy to reduce into CH_4, and results in a higher CH_4 evolution for the Pt–TiO_2 with MgO modified on its surface.[201]

It is worth noting that TiO_2 is a good model system in which the fundamental mechanisms of photocatalysis can be investigated. The wide bandgap of TiO_2 fundamentally limits its solar-energy conversion efficiency. Even though TiO_2 has been commercially used in air purifiers and self-cleaning windows, practical application in H_2 evolution and solar fuel conversion remains a big challenge. Therefore, further research and development in TiO_2-based materials are indispensable for exploring

sufficient functionality required from the industry. More importantly, the comprehensive investigation of TiO_2-based photocatalysis can provide scientists with valuable information for the study of other semiconductor photocatalysts, especially in the area of visible-light driven photocatalysis.

Acknowledgements

References

1 A. Hagfeldt and M. Gratzel, *Chem. Rev.*, 1995, **95**, 49–68.
2 M. R. Hoffmann, S. T. Martin, W. Y. Choi and D. W. Bahnemann, *Chem. Rev.*, 1995, **95**, 69–96.
3 T. L. Thompson and J. T. Yates, *Chem. Rev.*, 2006, **106**, 4428–4453.
4 H. Tong, S. X. Ouyang, Y. P. Bi, N. Umezawa, M. Oshikiri and J. H. Ye, *Adv. Mater.*, 2012, **24**, 229–251.
5 H. H. Chen, C. E. Nanayakkara and V. H. Grassian, *Chem. Rev.*, 2012, **112**, 5919–5948.
6 S. X. Ouyang and J. H. Ye, *J. Am. Chem. Soc.*, 2011, **133**, 7757–7763.
7 X. B. Chen, S. H. Shen, L. J. Guo and S. S. Mao, *Chem. Rev.*, 2010, **110**, 6503–6570.
8 S. Ouyang, H. Tong, N. Umezawa, J. Cao, P. Li, Y. Bi, Y. Zhang and J. Ye, *J. Am. Chem. Soc.*, 2012, **134**, 1974–1977.
9 Q. Xiang and J. Yu, *J. Phys. Chem. Lett.*, 2013, **4**, 753–759.
10 D. Y. C. Leung, X. Fu, C. Wang, M. Ni, M. K. H. Leung, X. Wang and X. Fu, *ChemSusChem*, 2010, **3**, 681–694.
11 D. Gust, T. A. Moore and A. L. Moore, *Acc. Chem. Res.*, 2009, **42**, 1890–1898.
12 S. N. Habisreutinger, L. Schmidt-Mende and J. K. Stolarczyk, *Angew. Chem., Int. Ed.*, 2013, **52**, 7372–7408.
13 W. Tu, Y. Zhou, Q. Liu, S. Yan, S. Bao, X. Wang, M. Xiao and Z. Zou, *Adv. Funct. Mater.*, 2013, **23**, 1743–1749.
14 R. Wang, K. Hashimoto, A. Fujishima, M. Chikuni, E. Kojima, A. Kitamura, M. Shimohigoshi and T. Watanebe, *Nature*, 1997, **388**, 431–432.
15 M. Gratzel, *Nature*, 2001, **414**, 338–344.
16 U. Bach, D. Lupo, P. Comte, J. E. Moser, F. Weissortel, J. Salbeck, H. Spreitzer and M. Gratzel, *Nature*, 1998, **395**, 583–585.
17 R. Asahi, T. Morikawa, T. Ohwaki, K. Aoki and Y. Taga, *Science*, 2001, **293**, 269–271.
18 S. U. M. Khan, M. Al-Shahry and W. B. Ingler, *Science*, 2002, **297**, 2243–2245.
19 H. G. Yang, C. H. Sun, S. Z. Qiao, J. Zou, G. Liu, S. C. Smith, H. M. Cheng and G. Q. Lu, *Nature*, 2008, **453**, 638–641.
20 X. B. Chen, L. Liu, P. Y. Yu and S. S. Mao, *Science*, 2011, **331**, 746–750.

This journal is © The Royal Society of Chemistry 2014

J. Mater. Chem. A, 2014, **2**, 12642–12661 | **12657**

21 M. Setvin, U. Aschauer, P. Scheiber, Y. F. Li, W. Y. Hou, M. Schmid, A. Selloni and U. Diebold, *Science*, 2013, **341**, 988–991.

22 X. Q. Chen, J. H. Ye, S. X. Ouyang, T. Kako, Z. S. Li and Z. G. Zou, *ACS Nano*, 2011, **5**, 4310–4318.

23 G. C. Xi, J. H. Ye, Q. Ma, N. Su, H. Bai and C. Wang, *J. Am. Chem. Soc.*, 2012, **134**, 6508–6511.

24 D. Chen and J. H. Ye, *Adv. Funct. Mater.*, 2008, **18**, 1922–1928.

25 W. T. Sun, Y. Yu, H. Y. Pan, X. F. Gao, Q. Chen and L. M. Peng, *J. Am. Chem. Soc.*, 2008, **130**, 1124–1125.

26 D. W. Jing and L. J. Guo, *J. Phys. Chem. B*, 2006, **110**, 11139–11145.

27 D. F. Wang, J. H. Ye, T. Kako and T. Kimura, *J. Phys. Chem. B*, 2006, **110**, 15824–15830.

28 S. X. Ouyang, H. Tong, N. Umezawa, J. Y. Cao, P. Li, Y. P. Bi, Y. J. Zhang and J. H. Ye, *J. Am. Chem. Soc.*, 2012, **134**, 1974–1977.

29 Z. G. Yi, J. H. Ye, N. Kikugawa, T. Kako, S. X. Ouyang, H. Stuart-Williams, H. Yang, J. Y. Cao, W. J. Luo, Z. S. Li, Y. Liu and R. L. Withers, *Nat. Mater.*, 2010, **9**, 559–564.

30 Y. Bi, S. Ouyang, N. Umezawa, J. Cao and J. Ye, *J. Am. Chem. Soc.*, 2011, **133**, 6490–6492.

31 Y. Wang, X. C. Wang and M. Antonietti, *Angew. Chem., Int. Ed.*, 2012, **51**, 68–89.

32 X. H. Li, X. C. Wang and M. Antonietti, *Chem. Sci.*, 2012, **3**, 2170–2174.

33 X. C. Wang, K. Maeda, A. Thomas, K. Takanabe, G. Xin, J. M. Carlsson, K. Domen and M. Antonietti, *Nat. Mater.*, 2009, **8**, 76–80.

34 K. G. M. Laurier, F. Vermoortele, R. Ameloot, D. E. De Vos, J. Hofkens and M. B. J. Roeffaers, *J. Am. Chem. Soc.*, 2013, **135**, 14488–14491.

35 X. L. Hu, C. Y. Sun, C. Qin, X. L. Wang, H. N. Wang, E. L. Zhou, W. E. Li and Z. M. Su, *Chem. Commun.*, 2013, **49**, 3564–3566.

36 T. R. Cook, Y. R. Zheng and P. J. Stang, *Chem. Rev.*, 2013, **113**, 734–777.

37 A. Fujishima and K. Honda, *Nature*, 1972, **238**, 37–38.

38 A. Fujishima, X. T. Zhang and D. A. Tryk, *Surf. Sci. Rep.*, 2008, **63**, 515–582.

39 X. Chen and S. S. Mao, *Chem. Rev.*, 2007, **107**, 2891–2959.

40 T. Watanabe, K. Hashimoto and A. Fujishima, *1st Int. Conf. TiO₂ Photocatalyst*, ed. H. A1-Ekabi, 1992.

41 H. Honda, A. Ishizaki, R. Soma, K. Hashimoto and A. Fujishima, *J. Illum. Eng. Soc.*, 1998, **27**, 42–49.

42 A. Fujishima, K. Hashimoto and T. Watanabe, *TiO₂ Photocatalysis, Fundamentals and Applications*, BKC, Tokyo, 1999.

43 K. Sunada, T. Watanabe and K. Hashimoto, *Environ. Sci. Technol.*, 2003, **37**, 4785–4789.

44 K. Hashimoto, H. Irie and A. Fujishima, *Jpn. J. Appl. Phys.*, 2005, **44**, 8269–8285.

45 C. F. Doodeve and J. A. Kitchener, *Trans. Faraday Soc.*, 1938, **34**, 902–908.

46 X. Pan, M.-Q. Yang, X. Fu, N. Zhang and Y.-J. Xu, *Nanoscale*, 2013, **5**, 3601–3614.

47 Y. Wang, Q. Wang, X. Zhan, F. Wang, M. Safdar and J. He, *Nanoscale*, 2013, **5**, 8326–8339.

48 M. A. Lazar and W. A. Daoud, *RSC Adv.*, 2013, **3**, 4130–4140.

49 J. R. Ran, J. Zhang, J. G. Yu, M. Jaroniec and S. Z. Qiao, *Chem. Soc. Rev.*, 2014, DOI: 10.1039/c3cs60425j.

50 L. Liu, Z. Liu, A. Liu, X. Gu, C. Ge, F. Gao and L. Dong, *ChemSusChem*, 2014, **7**, 618–626.

51 C. Aprile, A. Corma and H. Garcia, *Phys. Chem. Chem. Phys.*, 2008, **10**, 769–783.

52 R. Asahi, Y. Taga, W. Mannstadt and A. J. Freeman, *Phys. Rev. B: Condens. Matter*, 2000, **61**, 7459–7465.

53 J. I. L. Chen, G. von Freymann, S. Y. Choi, V. Kitaev and G. A. Ozin, *Adv. Mater.*, 2006, **18**, 1915–1919.

54 H. Li, Z. Bian, J. Zhu, D. Zhang, G. Li, Y. Huo, H. Li and Y. Lu, *J. Am. Chem. Soc.*, 2007, **129**, 8406–8407.

55 H. Xu, X. Q. Chen, S. X. Ouyang, T. Kako and J. H. Ye, *J. Phys. Chem. C*, 2012, **116**, 3833–3839.

56 H. Tong, N. Umezawa and J. H. Ye, *Chem. Commun.*, 2011, **47**, 4219–4221.

57 L. Q. Liu, S. X. Ouyang and J. H. Ye, *Angew. Chem., Int. Ed.*, 2013, **52**, 6689–6693.

58 X. Chen and C. Burda, *J. Am. Chem. Soc.*, 2008, **130**, 5018–5019.

59 T. Umebayashi, T. Yamaki, H. Itoh and K. Asai, *J. Phys. Chem. Solids*, 2002, **63**, 1909–1920.

60 J. F. Zhu, Z. G. Deng, F. Chen, J. L. Zhang, H. J. Chen, M. Anpo, J. Z. Huang and L. Z. Zhang, *Appl. Catal., B*, 2006, **62**, 329–335.

61 F. Gracia, J. P. Holgado, A. Caballero and A. R. Gonzalez-Elipe, *J. Phys. Chem. B*, 2004, **108**, 17466–17476.

62 M. H. Zhou, J. G. Yu and B. Cheng, *J. Hazard. Mater.*, 2006, **137**, 1838–1847.

63 D. W. Jing, Y. J. Zhang and L. J. Guo, *Chem. Phys. Lett.*, 2005, **415**, 74–78.

64 G. Colon, M. Maicu, M. C. Hidalgo and J. A. Navio, *Appl. Catal., B*, 2006, **67**, 41–51.

65 W. Ren, Z. Ai, F. Jia, L. Zhang, X. Fan and Z. Zou, *Appl. Catal., B*, 2007, **69**, 138–144.

66 S. Sato, R. Nakamura and S. Abe, *Appl. Catal., A*, 2005, **284**, 131–137.

67 J. C. Yu, J. G. Yu, W. K. Ho, Z. T. Jiang and L. Z. Zhang, *Chem. Mater.*, 2002, **14**, 3808–3816.

68 W. Q. Fang, X. L. Wang, H. M. Zhang, Y. Jia, Z. Y. Huo, Z. Li, H. J. Zhao, H. G. Yang and X. D. Yao, *J. Mater. Chem. A*, 2014, **2**, 3513–3520.

69 T. Ohno, M. Akiyoshi, T. Umebayashi, K. Asai, T. Mitsui and M. Matsumura, *Appl. Catal., A*, 2004, **265**, 115–121.

70 H. Xu, Z. Zheng, L. Zhang, H. Zhang and F. Deng, *J. Solid State Chem.*, 2008, **181**, 2516–2522.

71 G. R. Torres, T. Lindgren, J. Lu, C. G. Granqvist and S. E. Lindquist, *J. Phys. Chem. B*, 2004, **108**, 5995–6003.

72 B. Neumann, P. Bogdanoff, H. Tributsch, S. Sakthivel and H. Kisch, *J. Phys. Chem. B*, 2005, **109**, 16579–16586.

73 U. Koslowski, K. Ellmer, P. Bogdanoff, T. Dittrich, T. Guminskaya and H. Tributsch, *J. Vac. Sci. Technol., A*, 2006, **24**, 2199–2205.

74 L. K. Randeniya, A. B. Murphy and I. C. Plumb, *J. Mater. Sci.*, 2008, **43**, 1389–1399.

75 C. N. Zhang, S. H. Chen, L. Mo, Y. Huang, H. J. Tian, L. H. Hu, Z. P. Huo, S. Y. Dai, F. T. Kong and X. Pan, *J. Phys. Chem. C*, 2011, **115**, 16418–16424.

76 J. Y. Cao, Y. J. Zhang, H. Tong, P. Li, T. Kako and J. H. Ye, *Chem. Commun.*, 2012, **48**, 8649–8651.

77 J. Y. Cao, Y. J. Zhang, L. Q. Liu and J. H. Ye, *Chem. Commun.*, 2013, **49**, 3440–3442.

78 G. Liu, J. C. Yu, G. Q. Lu and H. M. Cheng, *Chem. Commun.*, 2011, **47**, 6763–6783.

79 S. Liu, J. Yu and M. Jaroniec, *Chem. Mater.*, 2011, **23**, 4085–4093.

80 J. Pan, G. Liu, G. M. Lu and H. M. Cheng, *Angew. Chem., Int. Ed.*, 2011, **50**, 2133–2137.

81 X. Zhao, W. Jin, J. Cai, J. Ye, Z. Li, Y. Ma, J. Xie and L. Qi, *Adv. Funct. Mater.*, 2011, **21**, 3554–3563.

82 H. Xu, S. Ouyang, P. Li, T. Kako and J. Ye, *ACS Appl. Mater. Interfaces*, 2013, **5**, 1348–1354.

83 S. Liu, J. Yu and M. Jaroniec, *J. Am. Chem. Soc.*, 2010, **132**, 11914–11916.

84 J. S. Chen, Y. L. Tan, C. M. Li, Y. L. Cheah, D. Luan, S. Madhavi, F. Y. C. Boey, L. A. Archer and X. W. Lou, *J. Am. Chem. Soc.*, 2010, **132**, 6124–6130.

85 H. Xu, P. Reunchan, S. X. Ouyang, H. Tong, N. Umezawa, T. Kako and J. H. Ye, *Chem. Mater.*, 2013, **25**, 405–411.

86 G. Liu, C. Sun, H. G. Yang, S. C. Smith, L. Wang, G. Q. Lu and H.-M. Cheng, *Chem. Commun.*, 2010, **46**, 755–757.

87 W.-J. Ong, L. L. Tan, S.-P. Chai, S.-T. Yong and A. R. Mohamed, *ChemSusChem*, 2014, **7**, 690–719.

88 Y. A. Vlasov, M. O'Boyle, H. F. Hamann and S. J. McNab, *Nature*, 2005, **438**, 65–69.

89 T. Baba, *Nat. Photonics*, 2008, **2**, 465–473.

90 G. Mie, *Ann. Phys.*, 1908, **330**, 377–445.

91 H. C. Hulst, *Light Scattering by Small Particles*, Dover, New York, 1981.

92 S. M. Scholz, R. Vacassy, J. Dutta and H. Hofmann, *J. Appl. Phys.*, 1998, **83**, 7860–7866.

93 M. Ren, R. Ravikrishna and K. T. Valsaraj, *Environ. Sci. Technol.*, 2006, **40**, 7029–7033.

94 X. Z. Zheng, S. G. Meng, J. Chen, J. X. Wang, J. J. Xian, Y. Shao, X. Z. Fu and D. Z. Li, *J. Phys. Chem. C*, 2013, **117**, 21263–21273.

95 J. D. Joannopoulos, P. R. Villeneuve and S. H. Han, *Nature*, 1997, **386**, 143–149.

96 A. Imhof, W. L. Vos, R. Sprik and A. Lagendijk, *Phys. Rev. Lett.*, 1999, **83**, 2942–2945.

97 M. Honda, T. Seki and Y. Takeoka, *Adv. Mater.*, 2009, **21**, 1801–1804.

98 J. I. L. Chen, G. von Freymann, V. Kitaev and G. A. Ozin, *J. Am. Chem. Soc.*, 2007, **129**, 1196–1202.

99 H. J. Koo, J. Park, B. Yoo, K. Yoo, K. Kim and N. G. Park, *Inorg. Chim. Acta*, 2008, **361**, 677–683.

100 H. Zeng, J. Li, J. P. Liu, Z. L. Wang and S. H. Sun, *Nature*, 2002, **420**, 395–398.

101 J. A. Fan, C. H. Wu, K. Bao, J. M. Bao, R. Bardhan, N. J. Halas, V. N. Manoharan, P. Nordlander, G. Shvets and F. Capasso, *Science*, 2010, **328**, 1135–1138.

102 S. A. Crooker, J. A. Hollingsworth, S. Tretiak and V. I. Klimov, *Phys. Rev. Lett.*, 2002, **89**, 186802.

103 R. Koole, P. Liljeroth, C. D. Donega, D. Vanmaekelbergh and A. Meijerink, *J. Am. Chem. Soc.*, 2006, **128**, 10436–10441.

104 H. Tong, N. Umezawa, J. H. Ye and T. Ohno, *Energy Environ. Sci.*, 2011, **4**, 1684–1689.

105 P. Wang, B. Huang, Y. Dai and M.-H. Whangbo, *Phys. Chem. Chem. Phys.*, 2012, **14**, 9813–9825.

106 Z. Wang, Y. Liu, B. Huang, Y. Dai, Z. Lou, G. Wang, X. Zhang and X. Qin, *Phys. Chem. Chem. Phys.*, 2014, **16**, 2758–2774.

107 M. Hu, J. Chen, Z.-Y. Li, L. Au, G. V. Hartland, X. Li, M. Marquez and Y. Xia, *Chem. Soc. Rev.*, 2006, **35**, 1084–1094.

108 A. Furube, L. Du, K. Hara, R. Katoh and M. Tachiya, *J. Am. Chem. Soc.*, 2007, **129**, 14852–14853.

109 Y. Nishijima, K. Ueno, Y. Yokota, K. Murakoshi and H. Misawa, *J. Phys. Chem. Lett.*, 2010, **1**, 2031–2036.

110 S. T. Kochuveedu, D. P. Kim and D. H. Kim, *J. Phys. Chem. C*, 2012, **116**, 2500–2506.

111 Y. Lin, C. X. Xu, J. T. Li, G. Y. Zhu, X. Y. Xu, J. Dai and B. P. Wang, *Adv. Optical Mater.*, 2013, **1**, 940–945.

112 R. A. Naphade, M. Tathavadekar, J. P. Jog, S. Agarkar and S. Ogale, *J. Mater. Chem. A*, 2014, **2**, 975–984.

113 M. Rycenga, C. M. Cobley, J. Zeng, W. Li, C. H. Moran, Q. Zhang, D. Qin and Y. Xia, *Chem. Rev.*, 2011, **111**, 3669–3712.

114 I. M. Arabatzis, T. Stergiopoulos, M. C. Bernard, D. Labou, S. G. Neophytides and P. Falaras, *Appl. Catal., B*, 2003, **42**, 187–201.

115 K. Awazu, M. Fujimaki, C. Rockstuhl, J. Tominaga, H. Murakami, Y. Ohki, N. Yoshida and T. Watanabe, *J. Am. Chem. Soc.*, 2008, **130**, 1676–1680.

116 P. Christopher, D. B. Ingram and S. Linic, *J. Phys. Chem. C*, 2010, **114**, 9173–9177.

117 H. Y. Li, W. B. Lu, J. Q. Tian, Y. L. Luo, A. M. Asiri, A. O. Al-Youbi and X. P. Sun, *Chem.–Eur. J.*, 2012, **18**, 8508–8514.

118 H. Eom, J. Y. Jung, Y. Shin, S. Kim, J. H. Choi, E. Lee, J. H. Jeong and I. Park, *Nanoscale*, 2014, **6**, 226–234.

119 A. Henglein, B. G. Ershov and M. Malow, *J. Phys. Chem.*, 1995, **99**, 14129–14136.

120 N. C. Bigall, T. Haertling, M. Klose, P. Simon, L. M. Eng and A. Eychmueller, *Nano Lett.*, 2008, **8**, 4588–4592.

121 R. Li, W. Chen, H. Kobayashi and C. Ma, *Green Chem.*, 2010, **12**, 212–215.

122 W. Zhai, S. Xue, A. Zhu, Y. Luo and Y. Tian, *ChemCatChem*, 2011, **3**, 127–130.

123 A. Marimuthu, J. Zhang and S. Linic, *Science*, 2013, **339**, 1590–1593.

124 Z. Y. Tan, D. W. Y. Yong, Z. H. Zhang, H. Y. Low, L. W. Chen and W. S. Chin, *J. Phys. Chem. C*, 2013, **117**, 10780–10787.

125 K. P. Rice, E. J. Walker, Jr, M. P. Stoykovich and A. E. Saunders, *J. Phys. Chem. C*, 2011, **115**, 1793–1799.

126 Y. J. Xiong, J. M. McLellan, J. Y. Chen, Y. D. Yin, Z. Y. Li and Y. N. Xia, *J. Am. Chem. Soc.*, 2005, **127**, 17118–17127.

This journal is © The Royal Society of Chemistry 2014

J. Mater. Chem. A, 2014, **2**, 12642–12661 | **12659**

127 Y. J. Xiong, B. Wiley, J. Y. Chen, Z. Y. Li, Y. D. Yin and Y. N. Xia, *Angew. Chem., Int. Ed.*, 2005, **44**, 7913–7917.

128 Y. J. Xiong, J. Y. Chen, B. Wiley, Y. N. Xia, Y. D. Yin and Z. Y. Li, *Nano Lett.*, 2005, **5**, 1237–1242.

129 S. Jung, K. L. Shuford and S. Park, *J. Phys. Chem. C*, 2011, **115**, 19049–19053.

130 S. Linic, P. Christopher and D. B. Ingram, *Nat. Mater.*, 2011, **10**, 911–921.

131 E. Hutter and J. H. Fendler, *Adv. Mater.*, 2004, **16**, 1685–1706.

132 X. M. Zhang, Y. L. Chen, R. S. Liu and D. P. Tsai, *Rep. Progr. Phys.*, 2013, **76**, 046401.

133 Y. Tian and T. Tatsuma, *J. Am. Chem. Soc.*, 2005, **127**, 7632–7637.

134 Y. Xia, Y. Xiong, B. Lim and S. E. Skrabalak, *Angew. Chem., Int. Ed.*, 2009, **48**, 60–103.

135 C. G. Silva, R. Juarez, T. Marino, R. Molinari and H. Garcia, *J. Am. Chem. Soc.*, 2011, **133**, 595–602.

136 Z. Zheng, B. Huang, X. Qin, X. Zhang, Y. Dai and M.-H. Whangbo, *J. Mater. Chem.*, 2011, **21**, 9079–9087.

137 Y. Q. Qu, R. Cheng, Q. Su and X. F. Duan, *J. Am. Chem. Soc.*, 2011, **133**, 16730–16733.

138 J. Lee, S. Mubeen, X. Ji, G. D. Stucky and M. Moskovits, *Nano Lett.*, 2012, **12**, 5014–5019.

139 S. Link, M. B. Mohamed and M. A. EI-Sayed, *J. Phys. Chem. B*, 1999, **103**, 3073–3077.

140 P. Salvador, *J. Appl. Phys.*, 1984, **55**, 2977–2985.

141 J. N. Wilson and H. Idriss, *J. Catal.*, 2003, **214**, 46–52.

142 K. Sivula, F. Formal and M. Gratzel, *ChemSusChem*, 2011, **4**, 432–449.

143 L. Kavan and M. Gratzel, *Electrochim. Acta*, 1995, **40**, 643–652.

144 M. Radecka and K. Zakrzewska, *J. Power Sources*, 2008, **181**, 46–55.

145 H. Maruka and A. Ghosh, *Sol. Energy Mater.*, 1978, **1**, 237.

146 J. Tauc, A. Abraham, L. Pajasova, R. Grigorovici and A. Vancu, *Non-Crystalline Solids*, North-Holland, Amsterdam, 1965.

147 P. Y. Yu and M. Cardona, *Fundamentals of Semiconductors: Physics and Materials Properties*, Springer, Heidelberg, edn 4, 2010.

148 U. Diebold, *Surf. Sci. Rep.*, 2003, **48**, 53.

149 T. L. Thompson and J. T. Yates Jr, *Chem. Rev.*, 2006, **106**, 4428.

150 H. G. Yang, G. Liu, S. Z. Qiao, C. H. Sun, Y. G. Jin, S. C. Smith, J. Zou, H. M. Cheng and G. Q. Lu, *J. Am. Chem. Soc.*, 2009, **131**, 4078–4083.

151 X. Han, Q. Kuang, M. Jin, Z. Xie and L. Zheng, *J. Am. Chem. Soc.*, 2009, **131**, 3152–3153.

152 S. W. Liu, J. G. Yu and M. Jaroniec, *Chem. Mater.*, 2011, **23**, 4085–4093.

153 M. Liu, L. Piao, W. Lu, S. Ju, L. Zhao, C. Zhou, H. Li and W. Wang, *Nanoscale*, 2010, **2**, 1115–1117.

154 W.-J. Ong, L.-L. Tan, S.-P. Chai, S.-T. Yong and A. R. Mohamed, *Nanoscale*, 2014, **6**, 1946–2008.

155 A. S. Barnard and L. A. Curtiss, *Nano Lett.*, 2005, **5**, 1261–1266.

156 B. H. Wu, C. Y. Guo, N. F. Zheng, Z. X. Xie and G. D. Stucky, *J. Am. Chem. Soc.*, 2008, **130**, 17563–17567.

157 J. Li and D. Xu, *Chem. Commun.*, 2010, **46**, 2301–2303.

158 J. Pan, X. Wu, L. Wang, G. Liu, G. Q. Lub and H.-M. Cheng, *Chem. Commun.*, 2011, **47**, 8361–8363.

159 N. Cuong Ky, H. G. Cha and Y. S. Kang, *Cryst. Growth Des.*, 2011, **11**, 3947–3953.

160 L. Wang, L. Zang, J. Zhao and C. Wang, *Chem. Commun.*, 2012, **48**, 11736–11738.

161 A. Vittadini, A. Selloni, F. P. Rotzinger and M. Gratzel, *Phys. Rev. Lett.*, 1998, **81**, 2954–2957.

162 A. Selloni, *Nat. Mater.*, 2008, **7**, 613–615.

163 S. W. Liu, J. G. Yu and M. Jaroniec, *J. Am. Chem. Soc.*, 2010, **132**, 11914–11916.

164 X. Y. Ma, Z. G. Chen, S. B. Hartono, H. B. Jiang, J. Zou, S. Z. Qiao and H. G. Yang, *Chem. Commun.*, 2010, **46**, 6608–6610.

165 X. G. Han, B. J. Zheng, J. J. Ouyang, X. Wang, Q. Kuang, Y. Q. Jiang, Z. X. Xie and L. S. Zheng, *Chem. Asian J.*, 2012, **7**, 2538–2542.

166 A. L. Linsebigler, G. Q. Lu and J. T. Yates, *Chem. Rev.*, 1995, **95**, 735–758.

167 M. Anpo, M. Che, B. Fubini, E. Garrone, E. Giamello and M. C. Paganini, *Top. Catal.*, 1999, **8**, 189–198.

168 R. Li, F. Zhang, D. Wang, J. Yang, M. Li, J. Zhu, X. Zhou, H. Han and C. Li, *Nat. Commun.*, 2013, **4**, 1432.

169 T. Ohno, K. Sarukawa and M. Matsumura, *New J. Chem.*, 2002, **26**, 1167–1170.

170 E. Bae and T. Ohno, *Appl. Catal., B*, 2009, **91**, 634–639.

171 E. Bae, N. Murakami and T. Ohno, *J. Mol. Catal. Chem.*, 2009, **300**, 72–79.

172 N. Murakami, Y. Kurihara, T. Tsubota and T. Ohno, *J. Phys. Chem. C*, 2009, **113**, 3062–3069.

173 M. D'Arienzo, J. Carbajo, A. Bahamonde, M. Crippa, S. Polizzi, R. Scotti, L. Wahba and F. Morazzoni, *J. Am. Chem. Soc.*, 2011, **133**, 17652–17661.

174 C. Di Valentin, G. Pacchioni and A. Selloni, *Phys. Rev. B: Condens. Matter*, 2004, **70**, 085116.

175 Z. S. Lin, A. Orlov, R. M. Lambert and M. C. Payne, *J. Phys. Chem. B*, 2005, **109**, 20948–20952.

176 J. B. Varley, A. Janotti and C. G. Van de Walle, *Adv. Mater.*, 2011, **23**, 2343–2347.

177 H. Irie, Y. Watanabe and K. Hashimoto, *J. Phys. Chem. B*, 2003, **107**, 5483–5486.

178 H. Fu, L. Zhang, S. Zhang, Y. Zhu and J. Zhao, *J. Phys. Chem. B*, 2006, 3061–3065.

179 T. Miyagi, M. Kamei, I. Sakaguchi, T. Mitsuhashi and A. Yamazaki, *Jpn. J. Appl. Phys.*, 2004, **43**, 775.

180 N. Umezawa and J. H. Ye, *Phys. Chem. Chem. Phys.*, 2012, **14**, 5924–5934.

181 A. Boonchun, N. Umezawa, T. Ohno, S. X. Ouyang and J. H. Ye, *J. Mater. Chem. A*, 2013, **1**, 6664–6669.

182 P. Reunchan, S. X. Ouyang, N. Umezawa, H. Xu, Y. J. Zhang and J. H. Ye, *J. Mater. Chem. A*, 2013, **1**, 4221–4227.

183 H. Yu, S. Ouyang, S. Yan, Z. Li, T. Yu and Z. Zou, *J. Mater. Chem.*, 2011, **21**, 11347–11351.

184 P. Reunchan, S. Ouyang, N. Umezawa, H. Xu, Y. Zhang and J. Ye, *J. Mater. Chem. A*, 2013, **1**, 4221–4227.

185 G. Xi, S. Ouyang and J. Ye, *Chem.–Eur. J.*, 2011, **17**, 9057–9061.

186 H. Xu, S. Ouyang, L. Liu, D. Wang, T. Kako and J. Ye, *Nanotechnology*, 2014, **25**, 165402.

187 J. Q. Liu, L. L. Ruan, S. B. Adeloju and Y. C. Wu, *Dalton Trans.*, 2014, **43**, 1706–1715.

188 S. Ho-Kimura, S. J. A. Moniz, A. D. Handoko and J. W. Tang, *J. Mater. Chem. A*, 2014, **2**, 3948–3953.

189 Y. Shiraishi, H. Sakamoto, Y. Sugano, S. Ichikawa and T. Hirai, *ACS Nano*, 2013, **7**, 9287–9297.

190 Y. Sugano, Y. Shiraishi, D. Tsukamoto, S. Ichikawa, S. Tanaka and T. Hirai, *Angew. Chem., Int. Ed.*, 2013, **52**, 5295–5299.

191 W. Schottky, *Z. Phys.*, 1939, **113**, 367–414.

192 Y. Nakato, K. Ueda, H. Yano and H. Tsubomura, *J. Phys. Chem.*, 1988, **92**, 2316–2324.

193 A. Tanaka, S. Sakaguchi, K. Hashimoto and H. Kominami, *ACS Catal.*, 2013, **3**, 79–85.

194 D. Tsukamoto, A. Shiro, Y. Shiraishi, Y. Sugano, S. Ichikawa, S. Tanaka and T. Hirai, *ACS Catal.*, 2012, **2**, 599–603.

195 Y. H. Hu, H. Wang and B. Hu, *ChemSusChem*, 2010, **3**, 782–796.

196 Q. Xiang, J. Yu and M. Jaroniec, *Nanoscale*, 2011, **3**, 3670–3678.

197 G. Lui, J.-Y. Liao, A. Duan, Z. Zhang, M. Fowler and A. Yu, *J. Mater. Chem. A*, 2013, **1**, 12255–12262.

198 W.-J. Ong, M. M. Gui, S.-P. Chai and A. R. Mohamed, *RSC Adv.*, 2013, **3**, 4505–4509.

199 J. G. Yu, T. T. Ma, G. Liu and B. Cheng, *Dalton Trans.*, 2011, **40**, 6635–6644.

200 J. Zhang, J. Yu, M. Jaroniec and J. R. Gong, *Nano Lett.*, 2012, **12**, 4584–4589.

201 S. J. Xie, Y. Wang, Q. H. Zhang, W. Q. Fan, W. P. Deng and Y. Wang, *Chem. Commun.*, 2013, **49**, 2451–2453.